PORT DOCUMENTATION PAGE

AD-A204 318

1b RESTRICTIVE MARKINGS
NONE

3 DISTRIBUTION / AVAILABILITY OF REPORT
Approved for public release.
Distribution unlimited.

4 PERFORMING ORGANIZATION REPORT NUMBER(S)
Technical Report No. 13

5 MONITORING ORGANIZATION REPORT NUMBER(S)

6a NAME OF PERFORMING ORGANIZATION
Massachusetts Institute of Technology

6b OFFICE SYMBOL (If applicable)

7a NAME OF MONITORING ORGANIZATION
ONR

6c ADDRESS (City, State, and ZIP Code)
77 Massachusetts Avenue, Room 1-306
Cambridge, MA 02139

7b ADDRESS (City, State, and ZIP Code)
800 North Quincy Street
Arlington, VA 22217

8a NAME OF FUNDING / SPONSORING ORGANIZATION
DARPA

8b OFFICE SYMBOL (If applicable)

9. PROCUREMENT INSTRUMENT IDENTIFICATION NUMBER
N00014-86-K-0768

8c ADDRESS (City, State, and ZIP Code)
1400 Wilson Boulevard
Arlington, VA 22209

10 SOURCE OF FUNDING NUMBERS

PROGRAM ELEMENT NO.	PROJECT NO.	TASK NO.	WORK UNIT ACCESSION NO.
R & T Code	A 400005		

11. TITLE (Include Security Classification)
A MOLECULAR DYNAMICS MODEL OF MELTING AND GLASS TRANSITION IN AN IDEALIZED TWO-DIMENSIONAL MATERIAL - I

12. PERSONAL AUTHOR(S) Deng, Derguo; Argon, Ali S.; and Yip, Sidney.

13a. TYPE OF REPORT	13b TIME COVERED	14. DATE OF REPORT (Year, Month, Day)	15. PAGE COUNT
Interim technical	FROM 1987 TO 1988	1989 January 23,	71

16. SUPPLEMENTARY NOTATION
Submitted for publication in Phi. Transactions of the Royal Society

17 COSATI CODES		
FIELD	GROUP	SUB-GROUP

18. SUBJECT TERMS (Continue on reverse if necessary and identify by block number)
Modeling melting and glass transition in two-dimensional material; computer simulation.

19. ABSTRACT (Continue on reverse if necessary and identify by block number)

In a preparatory study of structural relaxations and plastic flow in a two-dimensional idealized atomic glass, the process of melting and quenching through a glass transition has been studied by computer simulation using a molecular dynamics model. In this model, the transition from a solid to a melt was observed to take place when liquid-like structural elements composed of dipoles of 5 and 7 sided Voronoi polygons percolate through the two-dimensional structure of distorted hexagons in the form of strings. Such dipoles constitute discrete elements of excess free volume within which liquid like behavior is established in the sense of reduced cohesion or local elastic moduli. Upon quenching the melt, the percolation condition of liquid like regions is retained for under-cooled melts between the melting point and a glass transition temperature below which the percolation condition is broken and the thermal expansion is sharply reduced.

20 DISTRIBUTION / AVAILABILITY OF ABSTRACT
☒ UNCLASSIFIED/UNLIMITED ☐ SAME AS RPT ☐ DTIC USERS

21. ABSTRACT SECURITY CLASSIFICATION
Unclassified

22a NAME OF RESPONSIBLE INDIVIDUAL
Dr. JoAnn Millikan

22b TELEPHONE (Include Area Code)
(202) 696-4410

22c. OFFICE SYMBOL

DD FORM 1473, 84 MAR 83 APR edition may be used until exhausted.
All other editions are obsolete

SECURITY CLASSIFICATION OF THIS PAGE

A MOLECULAR DYNAMICS MODEL OF MELTING AND GLASS TRANSITION IN AN IDEALIZED TWO-DIMENSIONAL MATERIAL - (I)

D. Deng [1], A.S. Argon, and S. Yip

Massachusetts Institute of Technology, Cambridge, MA 02139, U.S.A.

Abstract

In a preparatory study of structural relaxations and plastic flow in a two-dimensional idealized atomic glass, the process of melting and quenching through a glass transition has been studied by computer simulation using a molecular dynamics model. In this model, the transition from a solid to a melt was observed to take place when liquid-like structural elements composed of dipoles of 5 and 7 sided Voronoi polygons percolate through the two dimensional structure of distorted hexagons in the form of strings. Such dipoles constitute discrete elements of excess free volume within which liquid like behavior is established in the sense of reduced cohesion or local elastic moduli. Upon quenching the melt, the percolation condition of liquid like regions is retained for under-cooled melts between the melting point and a glass transition temperature below which the percolation condition is broken and the thermal expansion is sharply reduced.

[1] On leave from the Institute for Precious Metals in Kunming, Yunnan Province, China.

The simulation which has used empirical pair potentials characteristic of Cu and Zr has substantially underpredicted the melting and glass transition temperatures and overpredicted the thermal expansion of Cu_xZr_{1-x} type glasses. These defects of the model can be attributed to the two-dimensional nature of the material, which stores larger concentrations of free volume than a corresponding three-dimensional material. In spite of these quantitative shortcomings, the model gives valuable insight into the topological features of the local atomic configurations at melting and upon vitrification.

I. INTRODUCTION

The modes of inelastic deformation in amorphous solids on the atomic scale below their glass transition temperatures, i.e., in their glassy behavior range, and how these are related to the structure of these solids, has been of fundamental interest. The approaches taken to elucidate these phenomena in amorphous metals, polymers, and network glasses have differed considerably along the traditionally different views taken by investigators in these fields. Nevertheless, these approaches have in general divided into two operationally different categories. In the first category are those studies that are based on kinematically acceptable, strain producing ad-hoc local mechanisms which involve cooperative atom or molecular segment motions, and which are constructed principally to model the inelastic shear resistance [1-9]. In the second category are mostly studies based on detailed computer simulations of the structure of atomic [10,11] (for a review see [12]) and polymeric [13,14] glasses, including some further analysis to explore the mechanisms of inelastic deformation in these simulated systems [15-17]. Related to the latter are studies [8,18,19] using analog models of two-dimensional atomic glasses based on the classical Bragg bubble model [20]. The various ad-hoc models and computer simulations have been necessary because of the difficulty of obtaining information by direct experimental methods on the very local structural alterations that occur in the inelastic deformation in glasses. Some investigators have pursued a different line of approach relating inelastic deformations in glasses to extensions of well defined mobile crystal defects, such as vacancies and dislocations (for a review see [2]). In our view,

however, these have not furnished many quantitatively useful explanations of either the topological features of the deformation process or its kinetics.

In this and the accompanying three communications (referred to as II-IV in what follows), we report the results of a series of computer simulations of the structure, its phase transitions, structural relaxations, and plastic deformation under stress of a two-dimensional model atomic glass. In these simulations, our goal was not to obtain quantitatively exact descriptions of structures, of physical processes of phase change, or of mechanical properties, results which can be compared directly with experimental data on metallic glasses. There are certain topological limitations of a two-dimensional simulation which does not permit this. Rather, our goal has been to elucidate complex topological processes of a cooperative nature, and to develop qualitative understanding and semi-quantitative scaling laws for them.

One principal objective of the study was the simulation of structural aging and the subsequent cooperative atom motions occurring in local shear transformations upon large strain shearing. To obtain the initial structures for these studies in glassy assemblies in a non-arbitrary way, it was decided to obtain all such initial states by melting and quenching the two-dimensional atom assemblies. In this communication, we discuss only our findings related to melting and the glass transition upon quenching.

In several instances, we have encountered significant constraints on the kinematics and the distributed nature of the processes of shear relaxation even in relatively large two-dimensional periodic cells, indicating the wisdom of preferring a large two-dimensional array of a fixed number of atoms, rather than

distributing them in a more confined but three-dimensional periodic cell – when the overall number could not be arbitrarily increased for reasons of tractability in the simulation – not to mention the difficulty in visualization of the local transformations.

II. DETAILS OF THE SIMULATION

2.1 The Atomic Potentials

The simulations reported here and in the accompanying communications make use of standard molecular dynamics (MD) simulation techniques [21]. In (MD) Newton's equations of motion for a two-dimensional system of N, particles are integrated using a fifth-order predictor-corrector algorithm. Periodic boundary conditions are imposed on the simulation cell, and through a Lagrangian formulation [22], the components of the basis vectors defining the cell are allowed to vary in accordance to any imbalance between the internal stress and an externally prescribed stress. The system temperature is defined in terms of the average kinetic energy of a particle. To maintain the system at a particular temperature, the particle velocities are rescaled at every time step of the simulation. If the system has reached thermal equilibrium, then the instantaneous temperature, without velocity rescaling, will fluctuate about a mean value which does not change in time.

The atomic interactions in the present simulations are given by pair potentials of the Lennard-Jones type [1] [10]:

$$\Phi(r_{ij}) = E_o \left[\left(\frac{r_o}{r_{ij}} \right)^m - \left(\frac{r_o}{r_{ij}} \right)^n \right] - a' r_{ij} + b' \qquad (1)$$

where $\Phi(r_{ij})$ is the potential energy of interaction between atoms i and j at a separation distance r_{ij}, r_o and E_o are length and energy parameters of the potential, and the constants a' and b' are chosen to obtain smooth truncation of the potential some place between the third and fourth nearest neighbors. The exponents m and n are phenomenologically assigned to obtain a desired form for the potential.

In our simulations, two different forms of the potential were used. In the early phase of the study of melting and stability of the quenched glassy state of a single component solid, a Lennard-Jones potential was used with $m = 12$, $n = 6$, $r_o = 3.405\mathring{A}$, and an energy to atomic mass ratio $E_o/m_o = 2.485\text{x}10^8\text{cm}^2/\text{sec}^2$, to give a fundamental atomic period $\eta = r_o\sqrt{m_o/E_o} = 2.16\text{x}10^{-12}\text{sec}$ ($\text{E}_\text{o} = 1.034\text{x}10^{-2}\text{eV}$, and $m_o = 6.656\text{x}10^{-23}\text{g}$). These particular parameter values are appropriate to the noble gas solid argon. The simulations were carried out under two constant external pressures: $p^* = 0$, and 1, in units of $\pi = E_o/r_o^3$ (= 41.9 MPA in 3-D), to explore the effect of pressure on structural stability. In a typical simulation run, the time step size has been taken at 1% of the fundamental period η, which makes it $2.16\text{x}10^{-14}$sec in this case. As we will

[1] For nomenclature of symbols, refer to the table at the end of this paper.

discuss below briefly, this single component solid crystallized exceedingly rapidly. Therefore, simulations with this system were not carried much further.

In the main simulation, which will be the subject of this and the accompanying communications, a modified Lennard-Jones potential of the type introduced by Kobayashi et al. [10] for a two-component glass, such as Cu_xZr_{1-x}, was used. For the system considered here, $x = 0.5$, $m = 8$, $n = 4$. The Cu and Zr atoms have been labelled as A and B respectively, and their characteristic parameters have been taken as follows: $r_o = 2.556\mathring{A}$, $m_o = 10.63\text{x}10^{-23}$g, $E_o = 0.15$eV for the Cu (A) atoms, giving a fundamental atomic period $\eta_A = 5.4\text{x}10^{-13}$sec, a fundamental stress unit $\pi_A = 1.437GPa$ (in 3-D). The interactions between the Zr atoms (B-B) and the Cu and Zr atoms (A-B) were obtained according to the following ratios: $r_{oBB}/r_o = 1.244$; $r_{oAB}/r_o = 0.5\ (1 + r_{oBB}/r_o) = 1.122$; $E_{oBB}/E_o = 1.94$; $E_{oAB}/E_o = E_{oBB}/E_o)^{1/2} = 1.393$. Furthermore, the two coefficients a' and b' were chosen such that interatomic forces vanish at a critical cut-off distance of $r_c = 2.5\ r_o$. The resulting pair potential for copper is shown in Fig. 1. The two other pair potentials look very similar. To enhance stability in this simulation, an external pressure of $p/\pi = 1.0$ was chosen (i.e., 1.437 GPa in 3-D). This is a substantial pressure, and its effect on the quantitative aspects of the simulation must be kept in mind. The time step size was taken at 5% of the fundamental period, i.e., at $1.1\text{x}10^{-14}$ sec.

The method by which the simulation cell is allowed to change volume and shape is based on a Lagrangian which contains a kinetic energy term associated with the motions of the cell vectors [22,23]. A mass parameter appears in this term; while it can be assigned any value, a proper choice is important because

it governs how quickly the cell vectors respond to the imbalances between the prescribed external pressure and the fluctuating internal pressure. We discuss the effect of this so-called wall mass on the simulations and its proper choice in Appendix I of the accompanying paper on structural relaxations, which we will refer to here as III [30]. The magnitude of this mass in the present simulation was 4.

2.2 Simulation Cell

The simulation cells that were chosen in this study contained 144 atoms initially arranged on a 12x12 grid in a hexagonal close packed pattern (see Fig. 9a). Because of the hexagonal symmetry, the simulation cell was 11.5% longer in the horizontal direction than in the vertical direction. Areas allocated to each atom were delineated by Voronoi polygons constructed in the conventional way. This was done under every circumstance, and proved to be of great value in visualization of distortions, but also in determination of strain increments at each atomic site and the level of coordination of atoms to their surroundings. To simulate properties of a two-dimensional solid of infinite extent in the plane of simulation, periodic boundary conditions were used throughout the simulations. In the simulations of the binary atom solids of $Cu_{0.5}Zr_{0.5}$, the Cu(A) and Zr(B) atoms were initially assigned randomly.

2.3 Melting and Quenching Simulations

The melting of the two-dimensional crystal lattice was achieved by step-wise increase of the system temperature. The dimensionless temperature $T^*(= T/\theta)$ was increased in steps that ranged from 0.025 to 0.1 (the normalized temperature $\theta = E_o/k$ is 120K for the one-component solid and 1739K for the two-component $Cu_{0.5}Zr_{0.5}$ solid). Between increments, the temperature was held constant by rescaling the particle velocities. To achieve equilibrium as defined by cumulative-averaged properties no longer changing with time, it was necessary to equilibrate for $3-4\text{x}10^3$ time steps at temperatures below the melting temperature and for $3-5\text{x}10^3$ time steps above the melting temperature. During the melting process, where large and discontinuous changes occur in the system, often more time steps were necessary to achieve stabilized melt structures. All temperature dependent intensive properties of the equilibrated system for the heating runs have been calculated after structural stability was attained at the new temperature, judged by an absence of further change in the average volume per atom. The same was done on cooling in the melt, down to where time dependent structural relaxations take progressively longer periods of time. In this case, the structural relaxations were only carried out partially for each cooling step to freeze in a structure typical of that of the subcooled melt. In this range, each temperature reduction of about 0.05 - 0.1 was followed by only 10^3 time steps of stabilization. Such quenching simulations amount to very high rates of cooling in the range of $3\text{x}10^{11}$K/sec for the one-component system and $3\text{x}10^{10}$K/sec for the two-component systems.

The atom coordinates for each state in the melting and quenching runs were stored for future use in relaxation studies.

III. RESULTS

3.1 Temperature Dependent Changes in Atomic Volume, Enthalpy, and Potential Energy

The changes in the average atomic volume (average Voronoi area) Ω^*, enthalpy per atom H^*, and potential energy per atom V^*, all in normalized units, resulting from the changes in system temperature have been determined for the melting and quenching runs for both the single-component solid under two pressures (0, 1.0), and the two-component solid under a pressure of 1.0, for each step of the runs.

The problem of relating the two-dimensional (2-D) results to three-dimensional (3-D) properties has been dealt with systematically as follows:

a. Stresses and pressures are defined for use in (3-D), but operationally are handled in intermediate level computations in (2-D), i.e., as forces per peripheral length. In final presentations, all results are normalized by the three-dimensional pressure unit (E_o/r_o^3) so the reader can determine (3-D) properties if desired.

b. All intensive properties of interest obtained from the simulation have been presented per atom when given in dimensioned units. In all other cases, they have been given in non-dimensional form, but still per atom.

Thus, the (2-D) simulation cell has been treated for (3-D) purposes, as if it had a thickness of r_o, although in every instance, the simulation was constrained to lie in a plane.

While the average Voronoi polygon area per atom Ω^* in units of the fundamental area r_o^2 is obtained directly from the simulation plane, the instantaneous potential energy per atom V^* and enthalpy per atom H^*, on a per atom basis were obtained as follows:

$$V^* = \frac{1}{nE_o} \sum_{i}^{n} \sum_{j \neq i}^{n} \frac{1}{2} \Phi(r_{ij}), \tag{2}$$

$$H^* = \frac{1}{nE_o} \sum_{i}^{n} \frac{1}{2} m_i v_i^2 + V^* + p\Omega^* \tag{3}$$

The results for Ω^*, H^*, and V^* are plotted as a function of T^* in Figs. 2 and 3 at two external pressures p^* of 0 and 1.0 (in units of $\pi = E_o/r_o^2$) for the single-component solid, and Fig. 4 for the two-component solid (constructed of equal numbers of atoms A and B) at an external pressure of 1.0.

In all cases, the properties, Ω^*, H^*, and V^* increase monotonically with increasing temperature. The changes in the properties of the one-component solid (Cases I and II), and the two-component solid (Case III) with increasing temperature are summarized in Table I, where α_o and α_m are the coefficients of linear thermal expansion at zero temperature and the melting point respectively. It can be seen that the ratio α_m/α_o is 6-9 for the one component solid and 2.5 for the two-component solid. Across the melting point, α does not increase significantly. The same is true for the rate of change of enthalpy and potential energy per atom. This suggests that the melting observed here is more a process of topological transition, and manifestations of a discontinuous behavior in the rates of change of intensive properties are weak. This conclusion will be reinforced later by inspection of the topological features associated with the melting process. The latter are to be expected because the limited system size and simulation durations make the observed transition necessarily smeared out.

The fractional linear expansion in these model solids upon melting range from about $2.14\text{x}10^{-2}$ for the one-component system to $5.49\text{x}10^{-3}$ for the two-component system, giving projected volumetric expansions on melting of $6.42\text{x}10^{-2}$ for the one-component solid and $1.65\text{x}10^{-2}$ for the two-component solid. These results do not compare too well with the known volume expansions of noble gas solids (12.7% for Ar) and close-packed metals (4.2% for Cu).

The absolute agreement in the melting points is also unsatisfactory. In the one-component solid, the melting point under no pressure is 42K and under a pressure of $p^* = 1.0$ (42 MPa) is 72K. Compared with the melting point of solid Argon of 84K at atmospheric pressure, both values are too low. The same is true

for the two-component solid, which at a pressure of $p^* = 1.0$ (1.437 GPa), has a melting point of 434K, while the melting point of the intermetallic compound $Cu_{0.5}Zr_{0.5}$ which it is to simulate, has a melting point of 1253K at atmospheric pressure.

It is worthwhile to note here that the phase diagram of the two-dimensional Lennard-Jones system has been studied by Monte Carlo simulation [24]. The triple point conditions are known to be $p_t^* = .815$, $T_t^* = .415$, and $p_t^* = .0056$. Since p_t^* is essentially zero, we can compare the melting temperature T_m^* and corresponding density ρ_m^* in Fig. 2 with these values. We find that $T_m^* = .353$ and $\rho_m^* = .812$. We believe that the reason why our T_m^* value is lower than the literature value is because our range cutoff r_c is somewhat shorter, and this effect is known to lower the melting point. In addition, we have not taken into account the long range correction to the pressure or correction for system size dependence.

The pressure dependence of the melting point, as simulated in our computations for the one-component solid is 11.3K/GPa. This is difficult to compare with actual experimental results, since the corresponding information is unavailable for noble gas solids. On a normalized basis, however, a comparison is possible where the result from the simulation $(\Delta T_m/T_m)/(\Delta P/\pi)$ is 0.526. The corresponding information for an alkali metal, such as Na is 0.338, where $\pi = (E_o/r_o^3)$ is taken as 0.65 GPa, as scaled down from the given ratio of Cu, on the basis of their different elastic properties. Clearly, the corresponding effect for a noble gas solid, such as Argon, should be larger and more comparable with our simulation.

From the information discussed above, we conclude that our simulation in 2-D underestimates the absolute melting points, but gives qualitatively acceptable results for the dependence of the melting point on pressure on a normalized basis. Furthermore, the results of the simulation on the linear coefficient of expansion for the two-component solid at $7.35 \times 10^{-5} K^{-1}$ at low temperatures is quite high when compared with what might be expected for $Cu_{0.5}Zr_{0.5}$, estimated to be about $1.1 \times 10^{-5} K^{-1}$ as an average for Cu and Zr, at equal volume fractions. This behavior of the simulation, however, is not unexpected, since 2-D models of disordered media are expected to give overestimates of specific volume and related properties, such as thermal expansion. Since the purpose of the simulation of melting was principally to obtain non-arbitrary starting coordinates for atoms in a disordered medium in the solid state upon quenching from the molten state, we do not attach too much importance to the relatively poor agreement between the results of the simulation and the absolute melting behavior. We will, however, find many points of interest in the topological features of the melt and its alterations upon quenching, as we will discuss these results below.

When the melt is cooled by systematically reducing the temperature in steps with intervening short periods of structural relaxation to achieve a condition of very slow change of properties (c.a. 1000 time steps), the intensive properties decrease continuously and monotonically. While the decreases above the melting temperature follow the same behavior of the heating curve, in reverse, this is not so below the melting point, as Figs. 2-4 clearly show. At these cooling rates, which are in the range of $10^{11} K sec^{-1}$, the liquid phase has no time to crystallize

by nucleation, but follows a temperature dependent contraction roughly parallel to that of the solid hexagonal close-packed phase, in an undercooled state, for the one and two component materials under pressure (Figs. 3 and 4). In the one-component material, the slope of the cooling curve always remains larger than that of the corresponding crystal, making the two curves meet before reaching zero temperature. This indicates that the one-component system under no pressure in the undercooled state is unstable and crystallizes even at these very high rates of quenching. In comparison, both the one-component system under pressure, as well as the two-component system under pressure, do not join onto the hexagonal crystal and remain at least quasi-stable in the disordered form.

In real systems, when a changeover occurs in the rates of change of intensive properties in a very narrow range of temperature from a liquid-like behavior to solid-like behavior, without any discontinuity in the property itself, the material is said to undergo a glass transition. This is indicated fairly clearly in Fig. 4 for the two-component material, where a glass transition is found at a normalized temperature of 0.18, in comparison to the melting point at 0.25.

There exist several simulation studies of the Lennard-Jones system adopted here. Monte Carlo results have been reported on melting in two dimensions [25], and on the glass transition in two dimensions in one and two component systems [26]. In three dimensions, molecular dynamics results on melting [27], crystallization [27], and glass transition [28] are available.

3.2 Changes in Topological Features

3.2.1 Radial distribution function (RDF)

The changes in the RDF of the three materials that occur upon heating are quite similar. In Figs. 5a-5d, we show the typical sequence for the two-component solid. At increasing temperatures, the peaks occur at larger distances and they become broader and less intense.

Two important qualitative changes occur in the RDF near the melting point. First, the second and third peaks, which are clearly separated in the expanded hexagonal close-packed structure below T_m merge together and form a very broad and short peak at $T > T_m$. This also occurs for the fourth and fifth peaks, which also spread out and fuse together in the melting process. Second, the clear separation between peaks present below T_m begins to be filled up near the melting point. This is particularly evident in the larger separation between the first and second, and between the third and fourth peaks. Thus, above the melting point, the RDF has non-zero values at all separations and the previously well defined first six peaks fuse into three broad and spread-out peaks. Some of these changes are also observable just below the melting point. This, as we have already pointed out is a result of the limited system size and short durations of the simulation which spreads out transitions.

The changes in the RDF at melting reflect the changes and smearing out of structural order. This is best followed from the ideal (2-D) hexagonal lattice

shown in Fig. 6 and its RDF reproduced immediately under it. Clearly, the second and third, and the fourth and fifth peaks are relatively close together, so that increased amplitude of thermal motion in the solid state and eventually the even larger amplitudes of atom motions possible in the molten state should smear out and fuse these peaks together.

The changes in the RDF upon quenching for the three materials are qualitatively different in the one-component solid from the two-component solid in the time range of the simulation. The one-component solid under no confining pressure crystallizes nearly completely, as Figs. 7a-7d show clearly. The same is also true under even a pressure of 1.0. In comparison, for the same quenching schedule, the two-component material under a pressure of 1.0 is much more stable and reaches a reasonably stable state at a temperature of 0.06, as Figs. 8a-8c show. Even here, however, as is seen in Fig. 8c, the second and third peaks have clearly begun to separate, and there are indications that the fifth peak is about to separate from the fourth peak. Nevertheless, the distribution is still continuous and without any breaks. We take this instantaneous state of well relaxed structure as a borderline case between a defective crystal and a glass with considerable topological short range order.

3.2.2 Topological changes in melting

The topological changes occurring in melting for the one-component and two-component systems under a normalized pressure of unity ($p^* = 1$) are shown in Figs. 9 and 10. The areas per atom are delineated by Voronoi polygons. Their

changing sizes, shapes, and associations reveal important details which cannot be perceived from the RDF.

In the sequences in Fig. 9, the changes in the one-component material are shown with increasing temperature. It must be born in mind that while each picture reflects the structure in near equilibrium after $1-4\text{x}10^3$ time steps, they are nevertheless only a snap shot in time, showing only one of a large number of statistically equivalent configurations with the same overall energy. Figure 9a shows the simulation cell of 144 atoms, which still shows a relatively well-ordered hexagonal atomic arrangement of the solid at half its melting point ($T^* = 0.3$). While all polygons are still hexagons at this temperature, careful inspection of these shows that some of them have acquired thermal motion induced small distortions. At a normalized temperature of 0.5 ($T = 0.83T_m$), all polygons are still hexagons, but many of them show quite large distortions. In Fig. 9b, at the melting point ($T_m^* = 0.6$) after only 1000 time steps before complete melting has occurred, qualitatively different topological changes are apparent. Now, most of the hexagons are quite visibly distorted, and many of the hexagons have been transformed into pentagons (5) and heptagons (7). Furthermore, accompanying the 5 and 7 sided polygons, corners sharing 4 edges also appear as a transient form for the first time. What is more, the 5 and 7 sided polygons show an affinity to each other. Figure 9c shows the structure at the melting point after 4000 time steps where structural equilibrium has been reached and no further expansion occurs. The simulation cell in the molten state has acquired a significant shear distortion without any applied shear stress. This can be traced to an artifact related to the smallness of the simulation cell. In a cell of amorphous material

of only 144 atoms subjected to a periodic boundary condition, the repetition in space of the borders of the cell constitutes a paracrystal in which the periodic border material makes up a significant volume fraction. This volume fraction can increase even further if the cell is allowed to shear in the liquid state, where the internal resistances to deformation have become very small. We ignore this distortion. More importantly, in the simulation cell of the molten material, a large number of the Voronoi polygons have now become 5 and 7 sided, indicated by the numbers in the polygons, and these have associated themselves in strings, in which 4 edged corners also appear frequently. In most instances, the strings percolate through the cell, as is shown in the bottom of Fig. 9c. At still higher temperatures, the percolating string-like association of the 5 and 7 sided polygons in the simulation cell become an even more prominent feature.

The corresponding distortions upon melting in the two-component material under a normalized pressure of unity ($p^* = 1$) are shown in the sequences in Fig. 10. In Fig. 10a, the initial hexagonal arrangement is shown at $T^* = 0.1(T = 0.4T_m)$. The Voronoi polygons containing the stiffer Zr atoms are identified by the small circles in the polygons. Because of the differences in size and local binding between the Cu and Zr atoms, many polygons appear already significantly distorted. Any apparent clustering of the Zr atoms in the simulation cell is illusory, since the Cu and Zr atoms were assigned to polygons purely randomly. At $T^* = 0.2(= 0.8T_m)$, again the hexagons show similarly increased distortions, as in the one-component material. Figure 10b shows the high temperature melt at $T^* = 0.3(T = 1.2T_m)$ with percolating strings of 5 and 7 sided polygons. At the same homologous temperature with respect to the

melting point, the departures from regularity of the hexagons are larger in the two-component system than in the one-component system.

We will demonstrate below that the 5 and 7 sided polygons usually associate themselves into a structural dipole of liquid-like material, and that the further percolating string-like associations of these dipoles imparts fluid-like behavior to the structure.

3.2.3 Topological changes in undercooled melts and in a glass transition

The topological changes in the arrangement of atoms undergoing quenching is shown in Fig. 11 for the two-component system, which is typical for all systems that were studied, including the one-component system. Figure 11a shows the two-component system at $T^* = 0.3(T = 1.2T_m)$ in the melt. A large and well-formed percolation string of 5 and 7 sided polygons is clearly visible. There are other broken strings of liquid-like polygon dipoles also visible, which can connect up to the main chain and thereby replace other segments of that chain by a statistically equivalent chain in other snapshots in time. Figure 11b shows the polygons in the simulation cell at $T^* = 0.2(T = 0.8T_m)$, which is an undercooled melt between T_m and T_g. A percolating string of liquid-like material is still evident in the figure. It is well to recall that the simulation involving stepwise lowering of the temperature followed by only 10^3 time steps for equilibration of the structure constitutes a quenching rate of about $10^{11} K sec^{-1}$. In Fig. 11c, the system is shown at $T^* = 0.14(= 0.78T_g = 0.56T_m)$, where many associated

dipoles of 5 and 7 sided polygons are visible, but the string-like percolation of these through the simulation cell is now broken. Thus, the material has apparently regained its solid-like behavior. Finally, in Fig. 11d, at a temperature of $T^* = 0.06 (= 0.33 T_g = 0.24 T_m)$, some 5 and 7 sided polygon dipoles still exist, but are now isolated in a background of short range ordered material. This represents the well-relaxed glassy state illustrated by the RDF in Fig. 8d.

IV. DISCUSSION

4.1 Melting and Glass Transition

Our simulation of two-dimensional hexagonal crystals has shown that in the first-order transition of melting, the system does not expand by spreading the disorder quasi-uniformly, but rather acquires well-defined imperfections having excess free volume. The principal ingredient of these imperfections are structural dipoles of associated Voronoi polygons of 5 and 7 sides.

When the system is molten so that solid-like behavior is replaced by liquid-like behavior, a critical concentration of the material must acquire a radically lowered level of cohesion. This occurs through the establishment of a percolation condition, in which strings of 5 and 7 sided polygon dipoles pervade the entire simulation cell in one or more directions and hence, through the periodic boundary conditions, reach over the entire infinite (2-D) space.

Clearly, for this picture to have meaning, the 5-7 dipole must have elemental liquid-like properties. That this is so, is shown in Fig. 12, which gives the average areas of the Voronoi polygons in units of r_o^2, of 5, 6, and 7 sides, as measured from actual simulation cells at a temperature of $T^* = 0.1$. These relative differences do not change much with temperature up to the melting point. As the figure shows, the average heptagon is about 10% larger than the average hexagon, which on the average is only 3% larger than the average pentagon. Thus, the area of the average dipole of 5-7 sided Voronoi polygons is about 7% larger than

a pair of average hexagons. Since the average hexagons themselves are about 9% larger at the melting point than the hexagons at $0°K$, the average dipole in the melt is about 16% larger than a pair of hexagons in a (2-D) material at rest at 0K. This is a substantial increase, which should put the material of the dipole at or beyond the decohesion strain, and give it indeed liquid-like properties. We show in the accompanying communications [29,31] (to be referred to here as (II) and (IV)) that both the structural relaxations and plastic deformation at low temperatures are strongly influenced by the liquid-like material.

The importance of such liquid-like material having excess free volume that percolates through the structure has been postulated earlier by Cohen and Grest [32,33] in relation to a glass transition and establishment of overall liquid-like behavior in bulk. Our simulations are in support of these views.

Our simulation has demonstrated further that glass transition takes place when in an undercooled melt, the percolation condition established by the strings of liquid-like material is broken. This view is also not entirely new, and while it has been set forth from time to time by others [see 36], it has not been widely favored.

A related and complementary concept, that of percolation of a property called rigidity, was developed independently at the same time by Phillips [34]. This was later quantified by Thorpe and formulated as a process known as vector percolation [35]. In this concept, one speaks of random networks consisting of floppy (or spongy) and rigid regions; isolated rings (polygons) with less than 6 sides would be rigid, while rings with 7 or more sides would be floppy. When rings become part of a network, the rigid rings remain rigid, but a floppy ring

now can become rigid if it is next to a rigid ring, and in this manner, rigidity can percolate through the network [35]. Although rigidity percolation was developed for network glasses, and has other applications to gellation, free volume percolation on the other hand is more pertinent to metallic glasses and the establishment of fluidity. We see, nevertheless, a certain analogy between these basic concepts and the percolation of structural dipoles observed in our simulation.

4.2 Topological Defects

The association of the 5 and 7 sided polygons into a structural dipole with a definite increment of free volume makes it a characteristic unit in the description of the molten state, as well as the glassy state in two-dimensional condensed matter. It is interesting that both in the molten state at the melting temperature, and in the glassy state below T_g, disorder in the material is not spread out uniformly over all volume elements. Rather, a considerable fraction of the material at any instance in time, maintains a reasonable degree of short range order while squeezing the disorder into the borders between the ordered regions, where it is accommodated in the form of the 5-7 sided structural dipoles. Thus, this arrangement must have a lower energy state than the one where atomic disorder is quasi-uniformly spread out over the entire (2-D) space. Clearly also, the 5-7 sided dipole cannot be rearranged into a pair of distorted 6 sided average polygons, since that would have a lower free volume, which apparently is prevented from becoming that by the constraint imposed by the surrounding regions of short range ordered material.

The 5-7 sided dipole of Voronoi polygons combining a region of excess dilatation and one with a smaller compaction would appear to have the features of an edge dislocation, and could readily be interpreted as such. To explore this possibility, we have analysed a number of well-defined lattice defects, such as single vacancies, di-vacancies, tri-vacancies, and tetra-vacancies, edge dislocations, and stacking faults that have been found in Bragg bubble rafts, which have the advantage of being readily available form the literature [37], and being fully equilibrated through an inter-bubble potential resembling closely certain inter-atomic potentials of metals [18]. Figure 13a-13d show respectively a vacancy, di-vacancy, tri-vacancy, and tetra-vacancy in bubble rafts, together with their Voronoi polygon representations. We see that in each case, these vacancy type clusters are delineated by a pair of 5-7 sided dipoles, in which the 7 sided Voronoi polygons face each other, and their interfaces with the 5 sided polygons are separated by from 1 to 4 intervening polygons. If the vacancies were aligned in a line, such arrangements can indeed be represented by a pair of edge dislocations with their tensile fields facing each other, terminating the rows of 1,2,3, and 4 vacancies. Figures 14a and 14b [37,38] show two edge dislocations in two bubble rafts with their associated Voronoi polygon descriptions. The dislocation in Fig. 14a is characterized by two adjoining 5 sided polygons facing two rather dilated 6 sided polygons across a common straight border, while the dislocation in Fig. 14b is represented by a dipole of 5 and 7 sided polygons. It is easy to demonstrate that if the dislocation in Fig. 14a is translated slightly toward the left or the right, one 5 sided polygon can be transformed into a distorted 6 sided polygon, while the large 6 sided polygon below the remaining 5 sided polygon

is transformed into a 7 sided polygon to look just like the dislocation in Fig. 14b. Figures 15a and 15b show two stacking faults in a bubble raft [37]. While the one in Fig. 15a is planar, and is terminated by two partial dislocations, the one in 15b is complex and distributed over a volume. Thus, in all of these instances, in the description of these crystal defects, edge dislocations play a role. When the dipoles occur in closely spaced pairs with the 7 sided polygons facing each other within one or two atomic positions, the defects are clearly of vacancy character in a perfect crystal environment, and an element of large free volume in an amorphous environment of distorted hexagons. Such defect pairs were found in significant concentrations in amorphous Bragg bubble rafts by Argon and Shi [19] as sets of closely spaced Burgers vector couples.

In the strings of percolating liquid-like material in the melt, subcooled melt, and the rapidly quenched glass, the 5-7 sided dipoles in touching configurations are predominantly ordered in sequences of 5-7-5-7, etc. This indicates that the material of the strings acts in the nature of a high angle grain boundary with the geometrically necessary dislocations being placed so close as to have their cores penetrate into each other. Thus, as is well known from the study of such high angle boundaries, their dislocation nature should then be completely lost, and their topological contents must be viewed as sets of polyhedra (polygons in 2-D)[39]. Hence, the structure of the melt consists of small islands of quasi-crystalline order separated by boundaries of quasi-periodically arranged polygons of 5-7 sides, retaining their topological signatures as stacked edge dislocation cores. As we will demonstrate in (II) [29], in the melt, the liquid-like material (boundary material) typically makes up a fraction of about 0.4 of the

total. Thus, the quasi-crystalline islands that are enclosed within the boundaries are exceedingly small indeed, and are internally somewhat disordered as well. It is interesting to note that the make-up of static amorphous Bragg soap bubble rafts composed of two dissimilar size bubbles and studied by Argon and co-workers [8,19] had structures very similar to the structure of the 2-D mats in the present simulations. In addition, the melting simulation carried out by Fukushima and Ookawa [37] by mechanically vibrating Bragg soap bubble rafts made up of bubbles of one size have also given melt structures that were remarkably similar to results of our simulation, even though in their case, the amplitudes of vibration were largely normal to the plane of the raft, rather than being in the plane.

The role of dislocations in melting and dislocation theories of melting are not new (for a discussion of some early attempts, see Nabarro [40]). Most of such developments were based on the observation that the energies of arrays of dislocations increase less than linearly, while the configurational entropy increases linearly, resulting in a well-defined discontinuous behavior at a definite temperature with a critical concentration of dislocation. Among the more modern studies is the computer simulation of Koizumi and Ninomiya [41], who have attained a glassy state by progressively increasing the density of screw dislocations of all types in a diamond cubic or f.c.c. lattice, followed by relaxing the positions of the atoms on the basis of an atomic pair potential. These authors have reported reaching RDFs that were quite similar to those obtained for amorphous metals, with total densities of dislocations in the range of $10^{14} - 10^{15}$ lines/cm^2, i.e., where the dislocation cores occupy nearly the entire volume. While these

authors do not report the final structure in more detail, they make the observation that core structures of dislocations remain intact in the final amorphous material. Similar results were reported also by Kotze and Kuhlmann-Wilsdorf [42].

The above observations bring to fore long standing controversies on the structure of the amorphous state and more particularly the role generalized dislocations could play in the inelastic deformation of such media (for a discussion, see Argon [43]). We will demonstrate in our associated simulation on plastic flow [31] (referred to earlier as (IV)) in the two-dimensional amorphous media, that while most of the inelastic deformation is assignable to local shear transformations occurring inside the liquid-like materials of the boundaries, a small component of strain also comes from mobility of dislocations in the quasi-crystalline domains encapsulated by the liquid-like material. As can be expected, this latter component of deformation assumes greater importance in well-relaxed glasses, with a high crystallinity where well-formed and isolated dis locations are readily recognizable inside the ordered region, as can be seen in Fig. 16 at sites A and B.

4.8 Generalization of Results

Although our observations of the thermo-physical properties of a two-dimensional idealized medium and its phase transitions qualitatively reproduce nearly all features that three-dimensional media exhibit, the results should be taken with some degree of caution. First, constraining the atoms to exist only

in two-dimensional mats prevents the local configurations from reaching lower energy forms by moving in all three directions. This invariably incorporates a higher free volume into the structure than is likely to be the case in three-dimensions, and may artificially enrich the liquid-like material. This must be one reason why the melting points found in our simulations were significantly lower and the coefficients of expansion higher than expected in comparison with three-dimensional material.

In three dimensions, we visualize the string-shaped percolation of the liquid-like material to take the form of tortuous boundaries pervading space and encapsulating small quasi-crystalline domains. The projection into three dimensions of closely spaced 5-7 sided polygons representing liquid-like material require replacing them with pairs of polyhedra of the type that make up high angle grain boundaries [39]. In well-relaxed glassy materials with a high degree of crystallinity, dislocation lines should exist, and can be of not only edge type, but also screw and of mixed nature. It is unlikely, however, that they play any more important role in the description of the structure or its phase transitions.

ACKNOWLEDGEMENT

The research described here has been supported from a number of sources. The initial simulations were made possible by a seed grant from the center for Materials Science and Engineering at M.I.T. from a parent NSF/MRL Grant DMR-84-18718. We are grateful to Director D. Litster for arranging this support. The later simulations were supported by NSF Grant DMR-85-17224 and the Advanced Research Projects Agency under a URI-Program under Contract N00014-86-K-0768. Additional salary support for DD throughout the entire period came from a post doctoral fellowship from the Allied Signal Corporation of Morristown, NJ, for which we are grateful to Dr. Lance Davis.

REFERENCES

1. J.J. Gilman, in "Dislocation Dynamics", edited by A.R. Rosenfield et al. (McGraw-Hill: New York), p. 3 (1968).

2. J.C.M. Li, in "Amorphous Metals and Semi Conductors", edited by P. Haasen and R.I. Jaffee (Pergamon Press: Oxford), p. 354 (1986).

3. A.S. Argon, Phil. Mag., 28, 39 (1973).

4. R.E. Robertson, J. Chem. Phys., 44, 3950 (1966).

5. P.B. Bowden and S. Raha, Phil. Mag., 22, 463 (1974).

6. F. Spaepen Acta Met., 25, 407 (1977).

7. A.S. Argon, Acta Met., 27, 47 (1979).

8. A.S. Argon and H.Y. Kuo, Mater. Sci. Eng., 39, 110 (1979).

9. A.S. Argon and L.T. Shi, in "Amorphous Materials: Modeling of Structure and Properties", edited by V. Vitek (A.I.M.E.: New York), p. 279 (1983).

10. S. Kobayashi, K. Maeda, and S. Takeuchi, J. Phys. Soc. Japan, 48, 1147 (1980).

11. K. Maeda and S. Takeuchi, J. Phys. F: Met. Phys., 12, 2767 (1982).

12. P.H. Gaskell, in "Glassy Metals II" - "Topics in Applied Physics", edited by H. Beck and H.-J. Guntherodt (Springer: Berlin), vol. 53, p. 5 (1983).

13. D. Theodorou and U.W. Suter, Macromolecules, 19, 139 (1986).

14. D. Theororou and U.W. Suter, Macromolecules, 19, 379 (1986).

15. S. Kobayashi, K. Maeda, and S. Takeuchi, Acta Met., 28, 164 (1980).

16. K. Maeda and S. Takeuchi, Phil. Mag., 44, 643 (1981).

17. D. Srolovitz, V. Vitek, and T. Egami, Acta Met., 31, 335 (1983).

18. L.T. Shi and A.S. Argon, Phil. Mag., A46, 255 (1982).

19. A.S. Argon and L.T. Shi, Phil. Mag., A46, 275 (1982).

20. W.L. Bragg and W.M. Lomer, Proc. Roy. Soc., A196, 171 (1949).

21. M.P. Allen and D.J. Tildeslay, "Computer Simulation of Liquids" (Clarendon Press: Oxford) (1987).

22. H.C. Andersen, J. Chem. Phys., 72, 2384 (1980).

23. M. Parrinello and A. Rahman, J. Appl. Phys., 52, 7182 (1981).

24. J.A. Barker, D. Henderson, and F.F. Abraham, Physica, 106A, 226 (1981), and references given therein.

25. F.F. Abraham, Rep. Prog. Phys., 45, 1149 (1982); J. Tobochnik and G.V. Chester, Phys. Rev., B25, 6778 (1982).

26. Y.J. Wang and G.V. Chester, Phys. Rev., B35, 3506 (1987).

27. S. Nose and F. Yonezawa, J. Chem. Phys., 84, 1803 (1985).

28. J.R. Fox and H.C. Andersen, J. Phys. Chem. 88, 4019 (1984); S. Nose and F. Yonezawa, Solid State Comm., 56, 1005 (1985).

29. D. Deng, A.S. Argon, and S. Yip (II), submitted to Acta Met..

30. D. Deng, A.S. Argon, and S. Yip, (III), submitted to Acta Met..

31. D. Deng, A.S. Argon, and S. Yip (IV), submitted to Acta Met..

32. M.H. Cohen and G.S. Grest, Phys. Rev., (B), 20, 1077 (1979).

33. G.S. Grest and M.H. Cohen, in "Advances in Chemical Physics", edited by T. Prigogine and S.A. Rice (Wiley: New York), vol. 48, p. 455 (1981).

34. J.C. Phillips, J. Non-Cryst. Sol., 34, 153 (1979); Ibid., 43, 37 (1981).

35. J.C. Phillips and M.F. Thorpe, Solid State Comm., 53, 699 (1985); M.F. Thorpe, J. Non-Cryst. Sol., 57, 355 (1983).

36. P. Meares, "Polymers: Structure and Bulk Properties" (Van Nostrand Reinhold Co.: London), Chapter 10, p. 251 (1965).

37. E. Fukushima and A. Ookawa, J. Phys. Soc. Japan, 10, 970 (1955).

38. F.A. McClintock and A.S. Argon, "Mechanical Behavior of Materials" (Addison Wesley: Reading, Mass.), p. 102 (1966).

39. M.F. Ashby, F. Spaepen, and S. Williams, Acta Met., 26, 1647 (1978).

40. F.R.N. Nabarro, "Theory of Crystal Dislocations" (Clarendon Press: Oxford), p. 688 (1967).

41. H. Koizumi and T. Ninomiya, J. Phys. Soc. Japan, 49, 1022 (1980).

42. I.A. Kotze and D. Kuhlmann-Wilsdorf, Phil. Mag., 23, 1133 (1971).

43. A.S. Argon, in "Dislocation Modeling of Physical Systems", edited by M.F. Ashby, et al. (Pergamon Press: Oxford), p. 393 (1981).

TABLE I

Melting and Solidification of Two-dimensional Model Solids

Case	p^*	$\pi/r_o(GPa)$	$\theta(K)$	T_m^*	T_g^*	$\alpha_o(K^{-1})$	$\alpha_m(K^{-1})$	$(\Delta\alpha/\alpha)_m$	$(\Delta H/H)$
1	0	0.0419	120	0.35	-	$6.62\text{x}10^{-4}$	$4.10\text{x}10^{-3}$	$2.14\text{x}10^{-2}$	-
2	1.0	0.0419	120	0.60	-	$2.83\text{x}10^{-4}$	$2.69\text{x}10^{-3}$	$2.43\text{x}10^{2}$	0.108
3	1.0	1.437	1739	0.25	0.19	$7.35\text{x}10^{-5}$	$1.85\text{x}10^{-4}$	$5.49\text{x}10^{-3}$	0.057

NOMENCLATURE

Dimensional Parameters

h_i	=	Enthalpy of atom i
k	=	Boltzmann's constant
m_o	=	Mass per atom
p_i	=	Pressure at atomic site i
r_{ij}	=	Distance between atoms i and j
r_o	=	Fundamental length scale in pair potential
S_i	=	Entropy of atom i
u_α	=	Displacement parallel to cartesian axis α
u_β	=	Displacement parallel to cartesian axis β
v_i	=	Velocity of atom i
x, y	=	Cartesian axes parallel to edges of undistorted simulation cell
$C(i)_{\alpha\beta\gamma\delta}$	=	Elastic constant defined at atomic site i
E_o	=	Energy scaling factor - binding energy in pair potential
H	=	Average enthalpy per atom
V	=	Average potential energy per atom
$S(i)_{\alpha\beta\gamma\delta}$	=	Elastic compliance defined at atomic side i
T	=	Absolute temperature
$\alpha, \beta, \gamma, \delta$	=	Cartesian axes in the plane of simulation usually referring to local atomic sites
$\gamma(i)_{xy}$	=	Total tangential shear strain at atomic site i
$\epsilon(i)_{xy}$	=	Total tensor strain at atomic site i
ρ	=	Density
$\sigma(i)_{xy}$	=	Tensor stress component at atomic site i
τ_i	=	Maximum shear stress (Mohr circle) at atomic site i
$\Phi(r_{ij})$	=	Energy potential between atom pairs i and j
Ω_o	=	Volume (Voronoi polygon area) per atom in reference crystal
Ω	=	Volume (Voronoi polygon area) per atom in disordered solid

Derived Units

m_o = Unit of mass
r_o = Unit of length
E_o = Unit of energy
ϕ = E_o/r_o, unit of force
ν = $\sqrt{E_o/m_o}$, unit of velocity
π = E_o/r_o^2, unit of (2-D) pressure or stress (generalized to E_o/r_o^3 in (3-D))
ρ_o = m/Δ_o, unit of density
θ = E_o/k, unit of temperature
η = $r_o\sqrt{m_o/E_o}$, unit of time

Normalized Quantities

p^* = p/π, dimensionless pressure
v^* = v/ν, dimensionless velocity
E^* = Φ/E_o, dimensionless energy
F^* = F/ϕ, dimensionless force
T^* = T/θ, dimensionless temperature
ρ^* = ρ/ρ_o, dimensionless density
σ^*_{xy} = σ_{xy}/π, dimensionless tensor stress element
τ^* = τ/π, dimensionless maximum shear stress
Ω^* = Ω/Ω_o, dimensionless atomic volume

FIGURE CAPTIONS

Fig. 1 The interatomic pair potential between Cu atoms used in the simulation with the two-component $Cu - Zr$) material.

Fig. 2 Temperature variations of dimensionless volume Ω^*, enthalpy H^*, and potential energy V^*, all on a per atom basis for the one-component model at external pressure of $p^* = 0$. Heating and cooling results are denoted by squares and circles respectively.

Fig. 3 Same as Fig. 2, except $p^* = 1.0$.

Fig. 4 Same as Fig. 3, except the system is the two-component $(Cu - Zr)$ model.

Fig. 5 Temperature dependent alterations in the RDF in the two-component material upon heating at $p^* = 1.0$: (a) $T^* = 0.05$, (b) $T^* = 0.225$, (c) $T^* = 0.25$ $(T = T_m)$, and (d) $T^* = 0.3$.

Fig. 6 The RDF peak positions in a perfect hexagonal structure.

Fig. 7 The temperature dependent alterations in the RDF in the one-component material upon quenching at $p^* = 0$: (a) $T^* = 0.35$, (b) $T^* = 0.25$ $(T = T_m)$, (c) $T^* = 0.15$, and (d) $T^* = 0.05$.

Fig. 8 Temperature dependent alterations in the RDF in the two-component material below the melting point at an external pressure of $p^* = 1.0$: (a) $T^* = 0.24$, (b) $T^* = 0.14$, and (c) $T^* = 0.06$.

Fig. 9 Temperature dependent alterations in the structure of the one-component material upon heating at an external pressure of $p^* = 1.0$: (a) $T^* = 0.3$ $(T = 0.5T_m)$, (b) $T^* = 0.6$ $(T = T_m)$,

incomplete melting after only 10^3 time steps, and
(c) $T^* = 0.6$ ($T = T_m$), complete melting
after 4000 time steps.

Fig. 10 Temperature dependent alterations in the structure of the two-component material upon heating at an external pressure of $p^* = 1.0$: (a) $T^* = 0.1$, the dark atoms are Zr, the light ones Cu, (b) $T^* = 0.3$ ($T = 1.2T_m$) after complete melting the 5 and 7 sided polygons associate into percolating strings that traverse across the cell.

Fig. 11 Temperature dependent alterations in the structure of the two-component material upon quenching at an external pressure of $p^* = 1.0$: (a) $T^* = 0.3$ ($T = T_m$), (b) $T^* = 0.2$ ($T_g < T < T_m$), (c) $T^* = 0.14$ ($T < T_g$), and (d) $T^* = 0.06$.

Fig. 12 Dependence of the average volume of the Voronoi polygons on the number of sides of the polygons, in the two-component material at $T^* = 0.1$.

Fig. 13 Distortions produced in the Voronoi polygon field of a perfect hexagonal buble raft produced by specific vacancy clusters: (a) vacancy, (b) di-vacancy, (c) tri-vacancy, and (d) tetra-vacancy.

Fig. 14 Distortions produced in the Voronoi polygon field of a perfect hexagonal buble raft produced by edge dislocations: (a) edge dislocation in an intermediate position between two low energy configurations, and (b) edge dislocation in the low energy configuration.

Fig. 15 (a) A stacking fault with two terminating partials in a perfect hexagonal bubble raft, and (b) a complex two-dimensional fault.

Fig. 16 Some isolated edge dislocations (5-7 sided dipoles) in a well relaxed two-component glass.

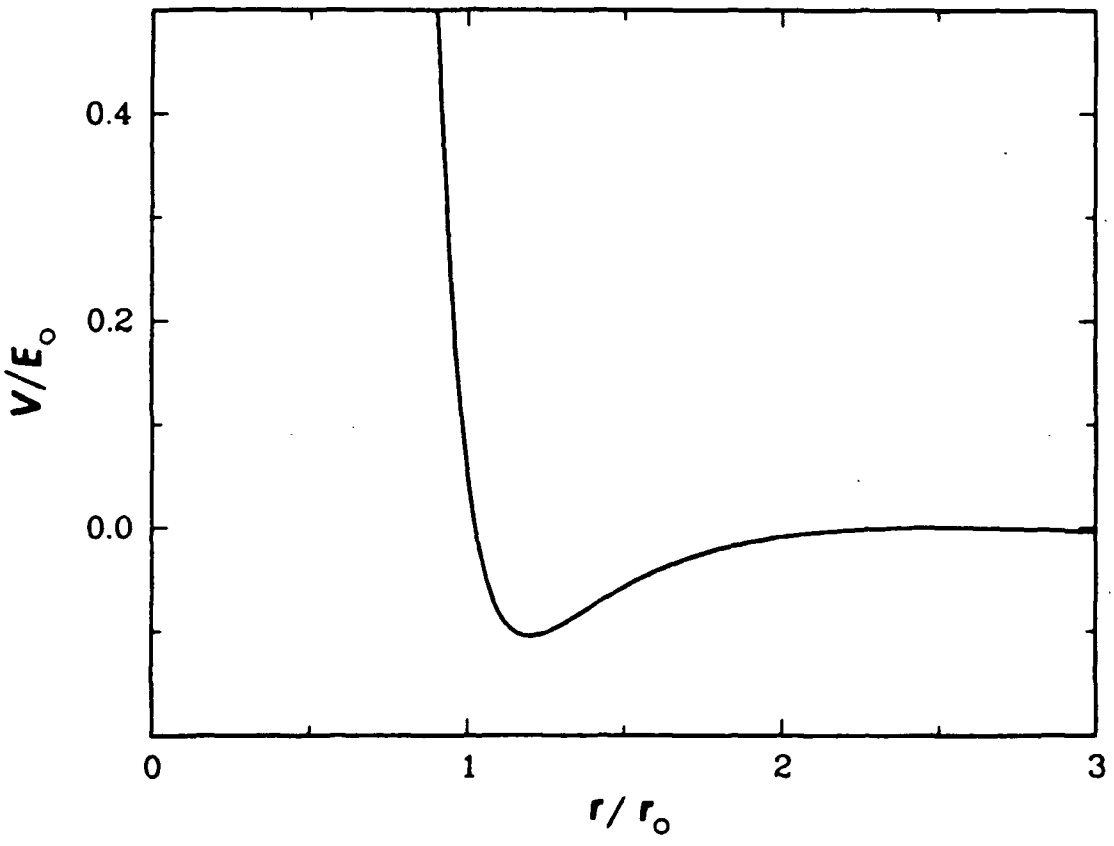

Fig. 1 - The interatomic pair potential between Cu atoms used in the simulation with the two-component (Cu-Zr) material.

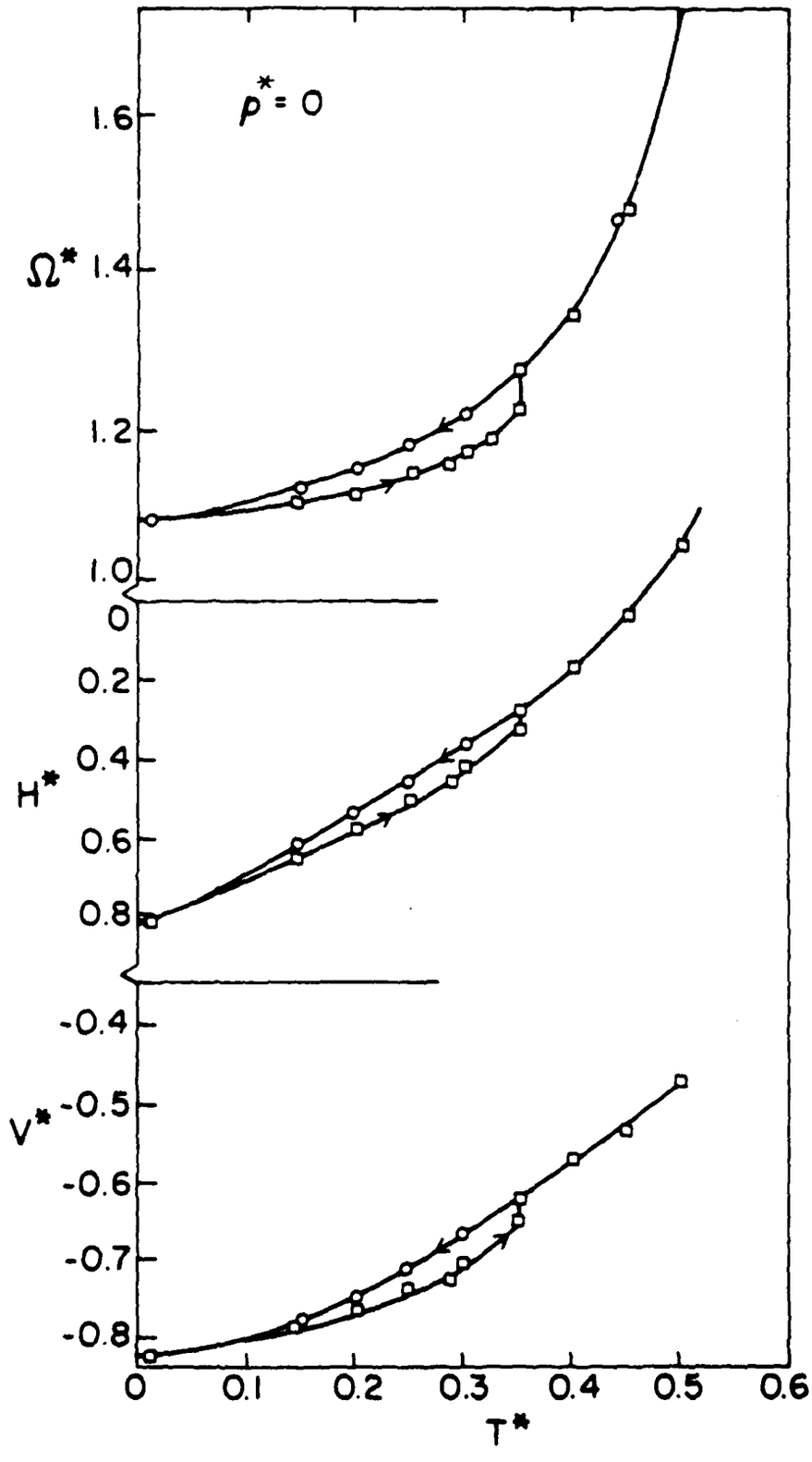

Fig. 2 - Temperature dependent changes in the Volume per atom Ω^*, enthalpy per atom H^*, and potential energy per atom V^*, all in normalized units for the one-component material under an external pressure of $p^* = 0$.

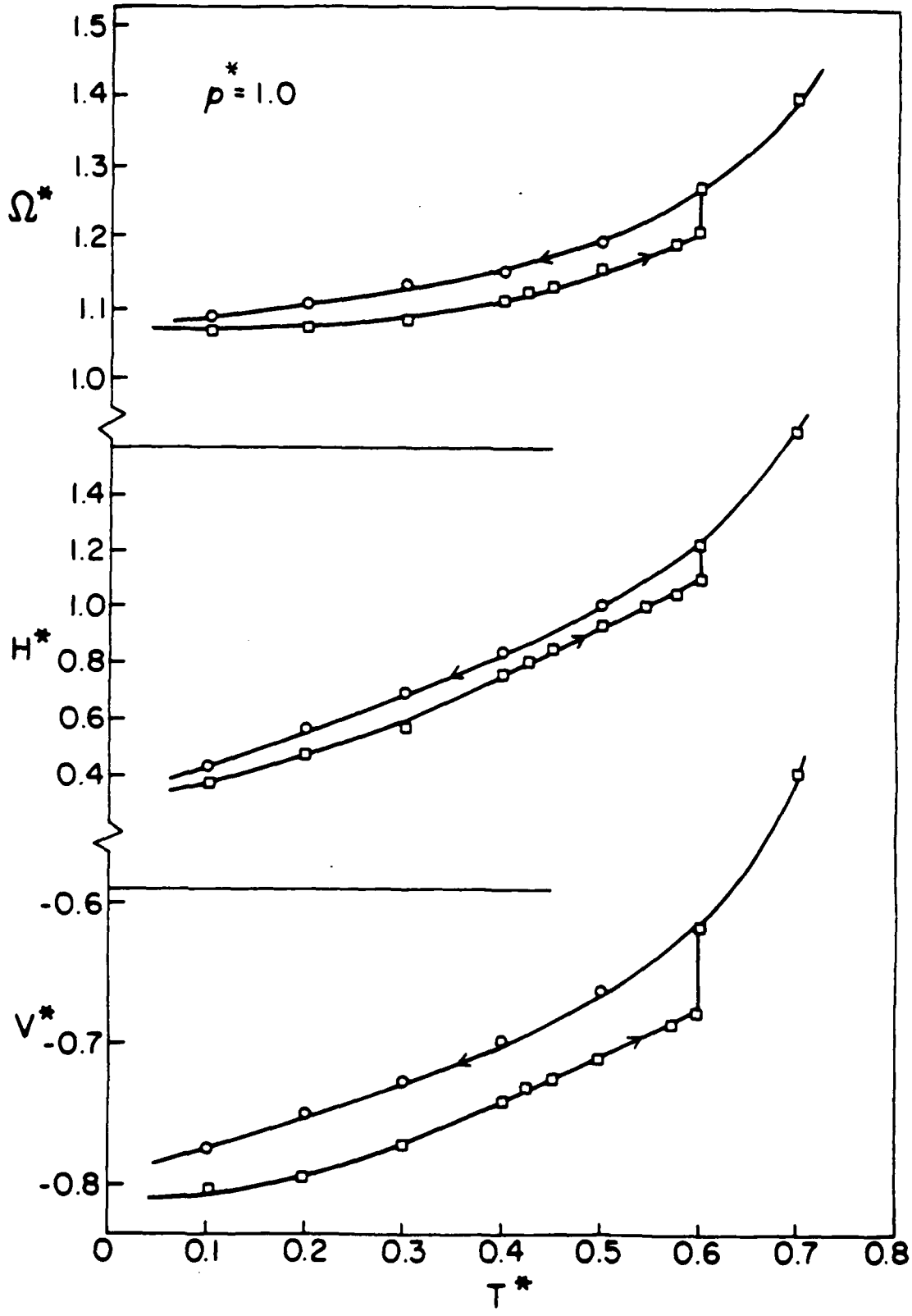

Fig. 3 - Temperature dependent changes in the volume per atom Ω^*, enthalpy per atom H^*, and potential energy per atom V^*, all in normalized units for the one-component material under an external pressure of $p^* = 1.0$.

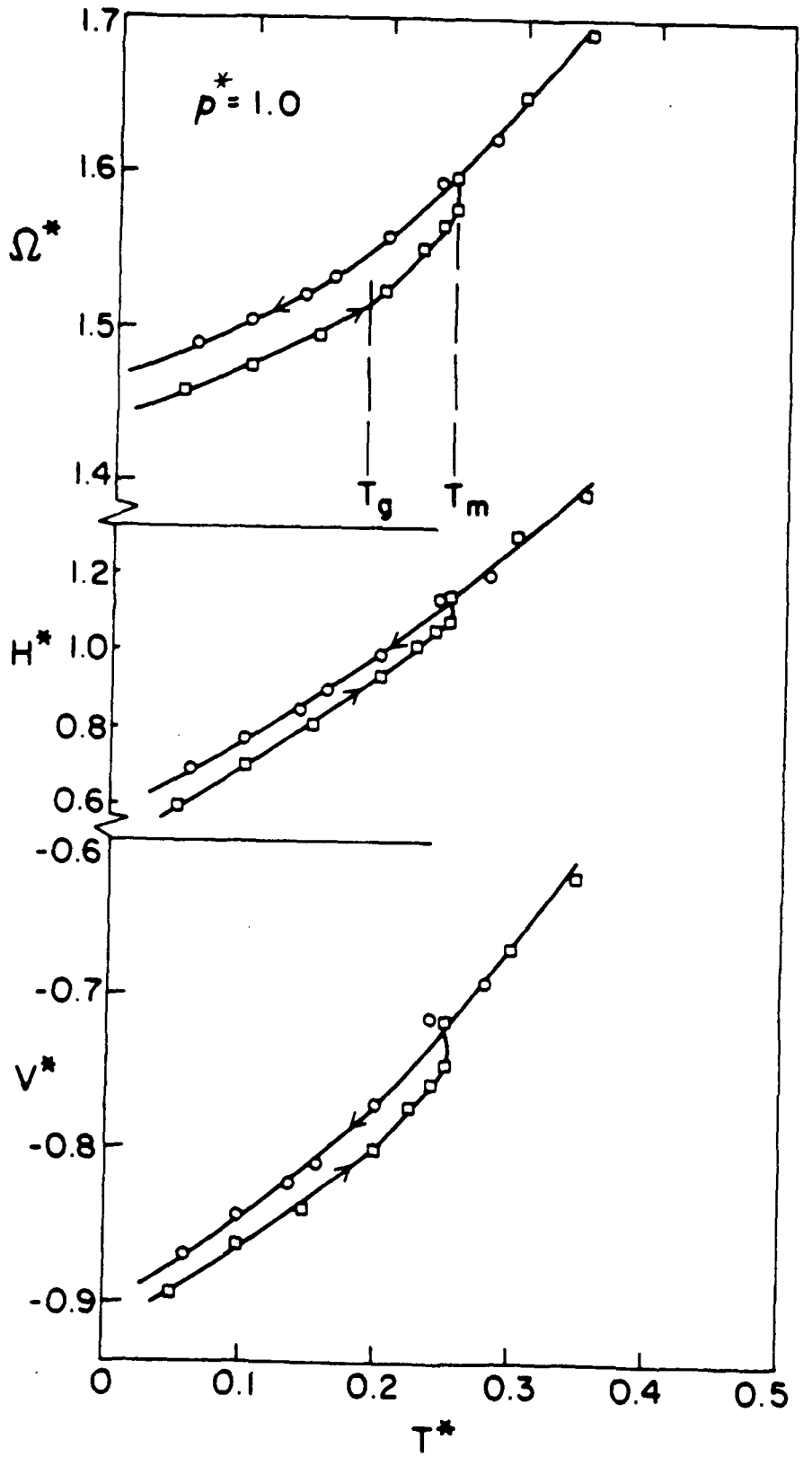

Fig. 4 - Temperature dependent changes in the volume per atom Ω^*, enthalpy per atom H^*, and potential energy per atom V^*, all in normalized units for the two-component (Cu-Zr) material under an external pressure of $p^* = 1.0$.

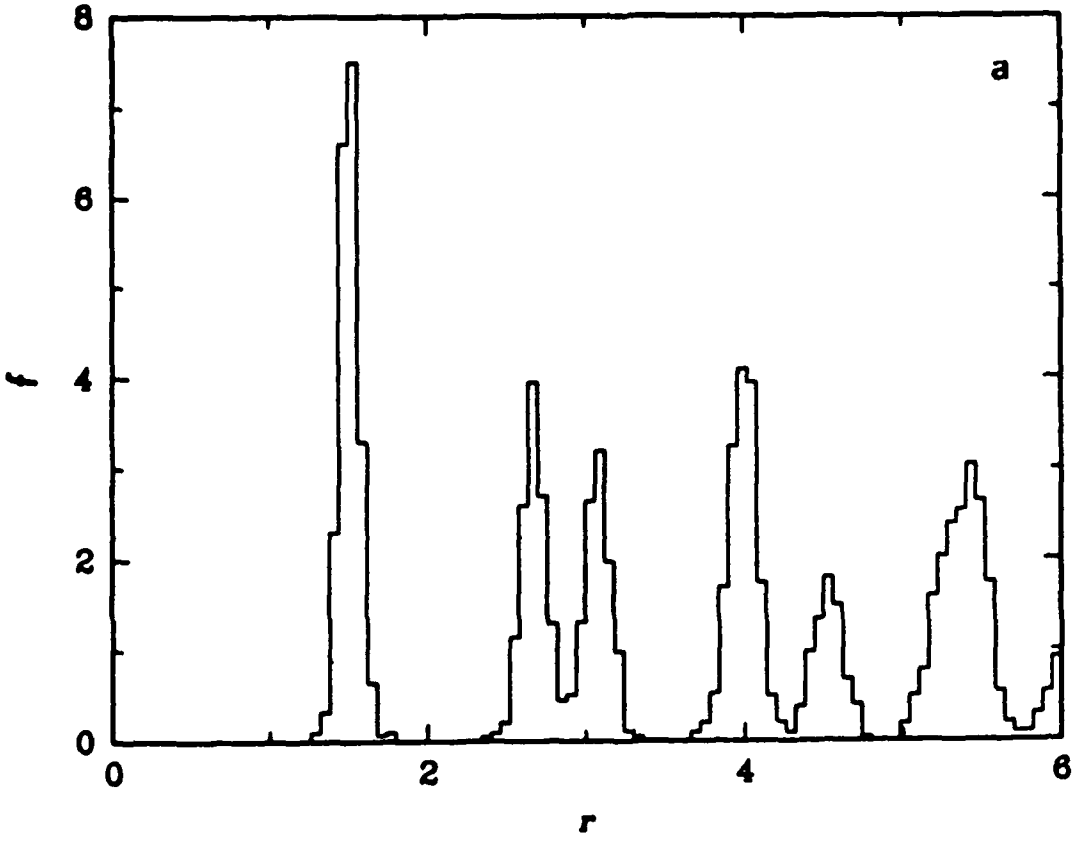

Fig. 5 - Temperature dependent alterations in the RDF in the two-component material upon heating at $p^* = 1.0$: (a) $T^* = 0.05$, (b) $T^* = 0.225$, (c) $T^* = 0.25$ ($T = T_m$), and (d) $T^* = 0.3$.

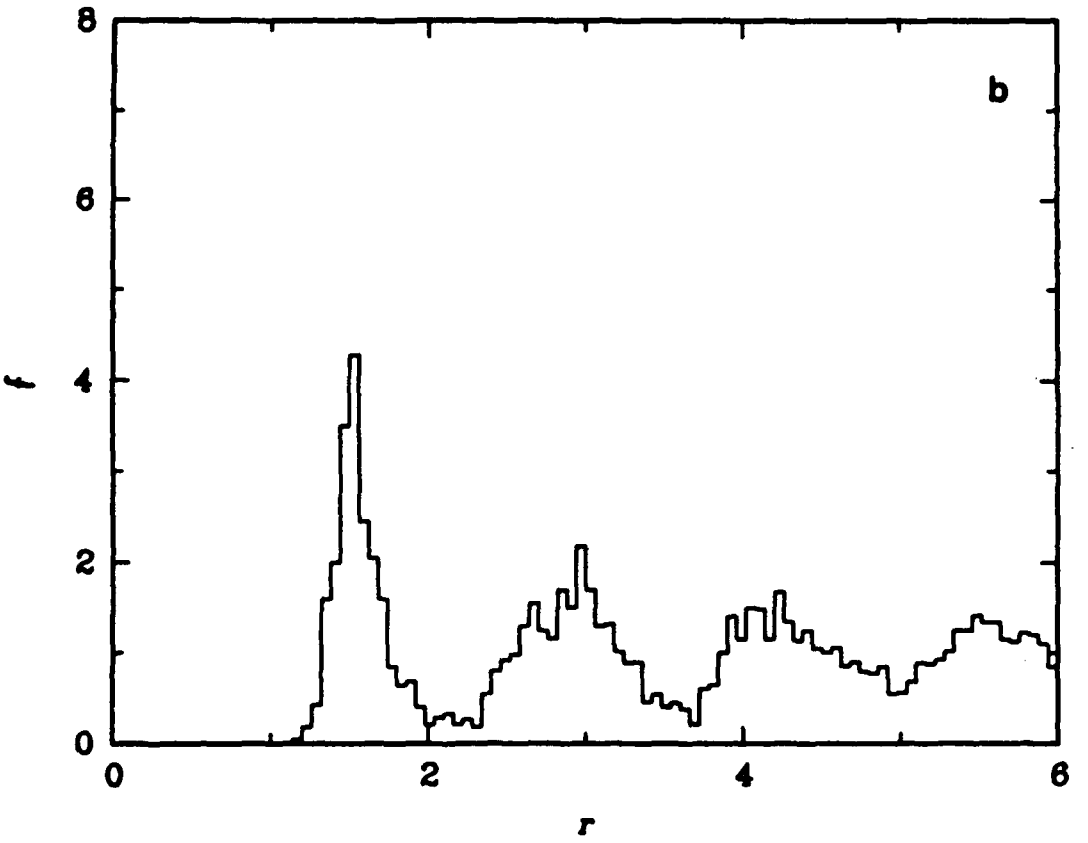

Fig. 5b

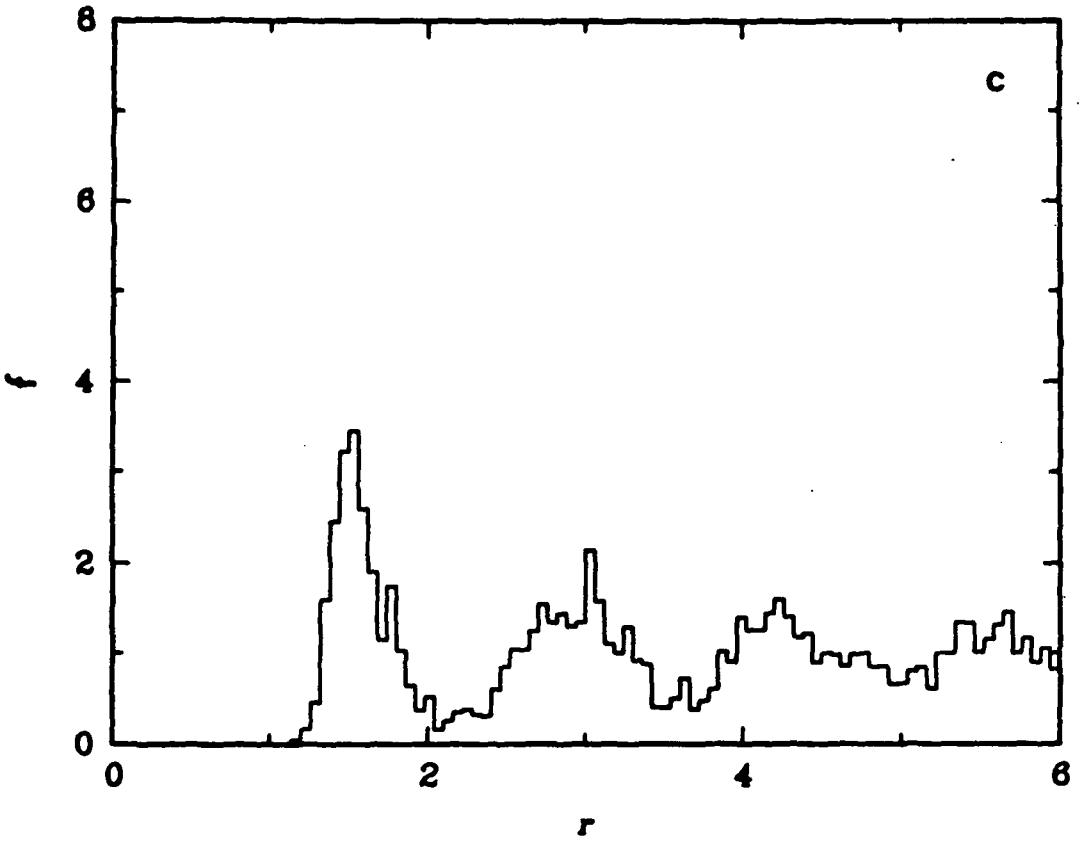

Fig. 5c

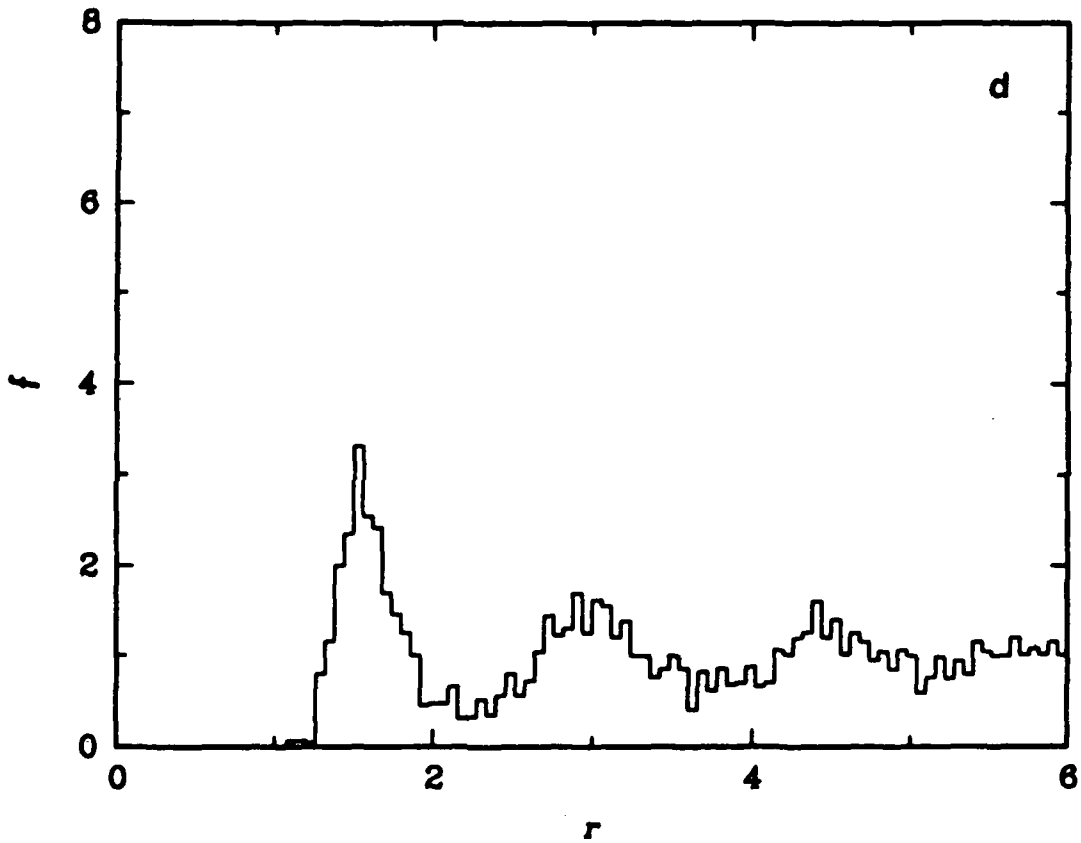

Fig. 5d

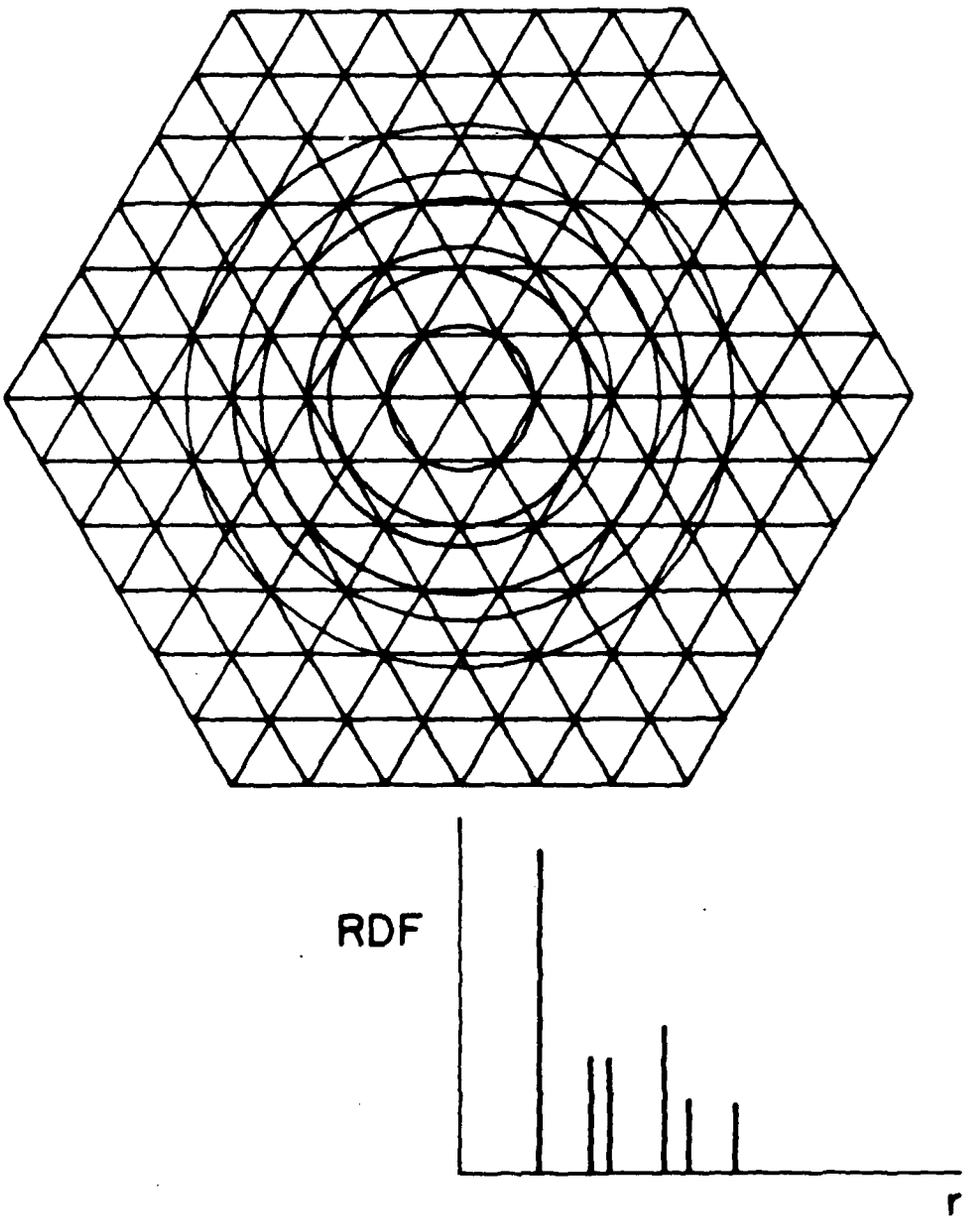

Fig. 6 - The RDF peak positions in a perfect hexagonal structure.

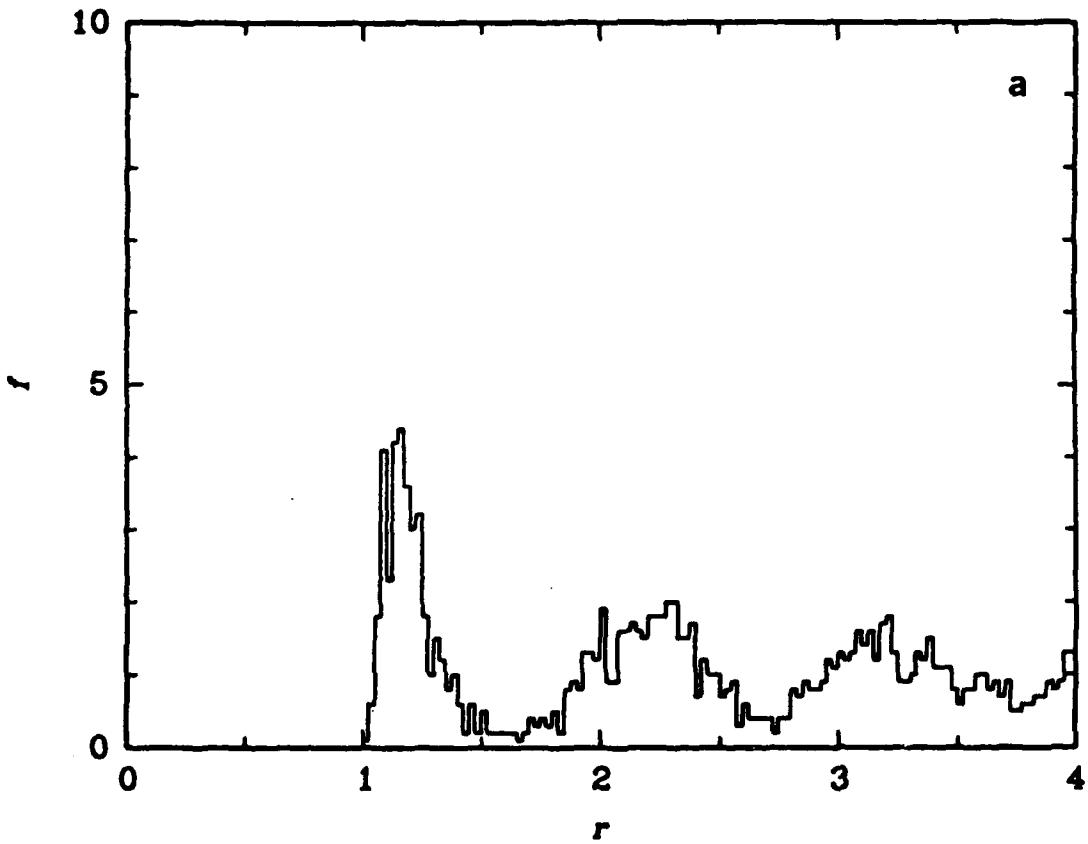

Fig. 7 - The temperature dependent alterations in the RDF in the one-component material upon quenching at $p^* = 0$: (a) $T^* = 0.35$, (b) $T^* = 0.25$ ($T = T_m$), (c) $T^* = 0.15$, and (d) $T^* = 0.05$.

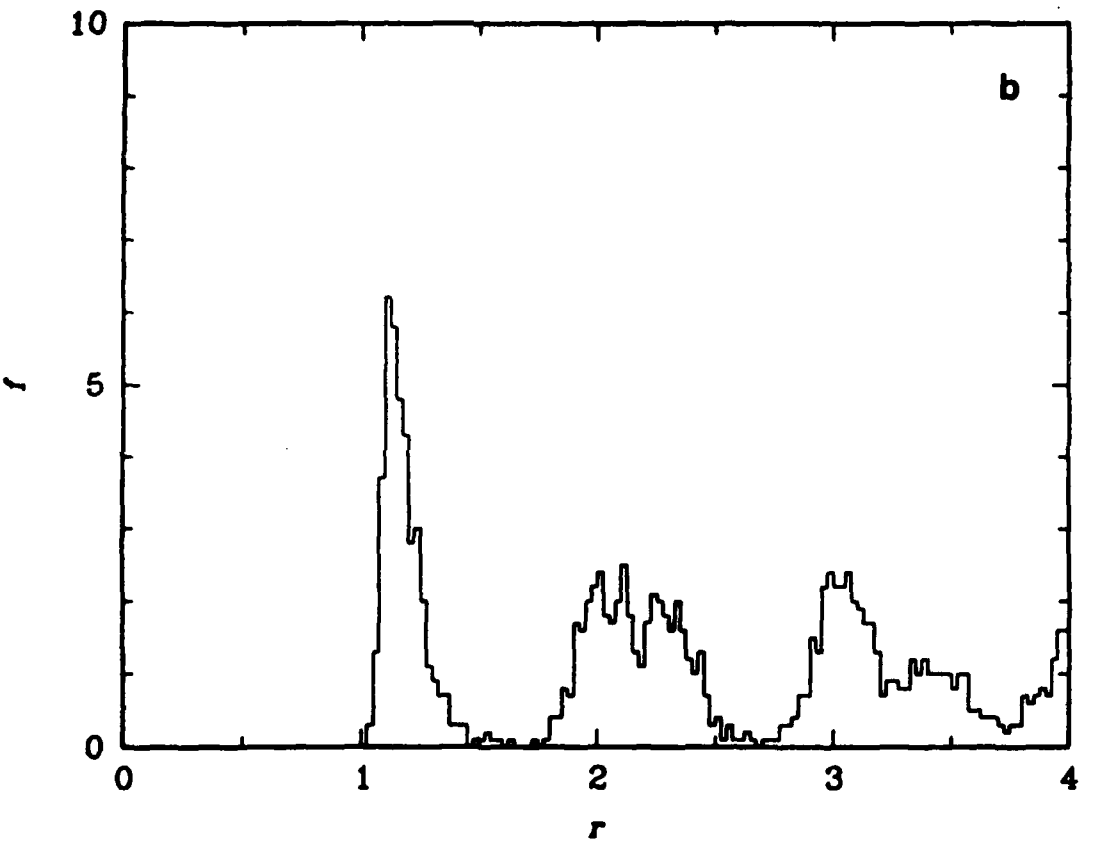

Fig. 7b

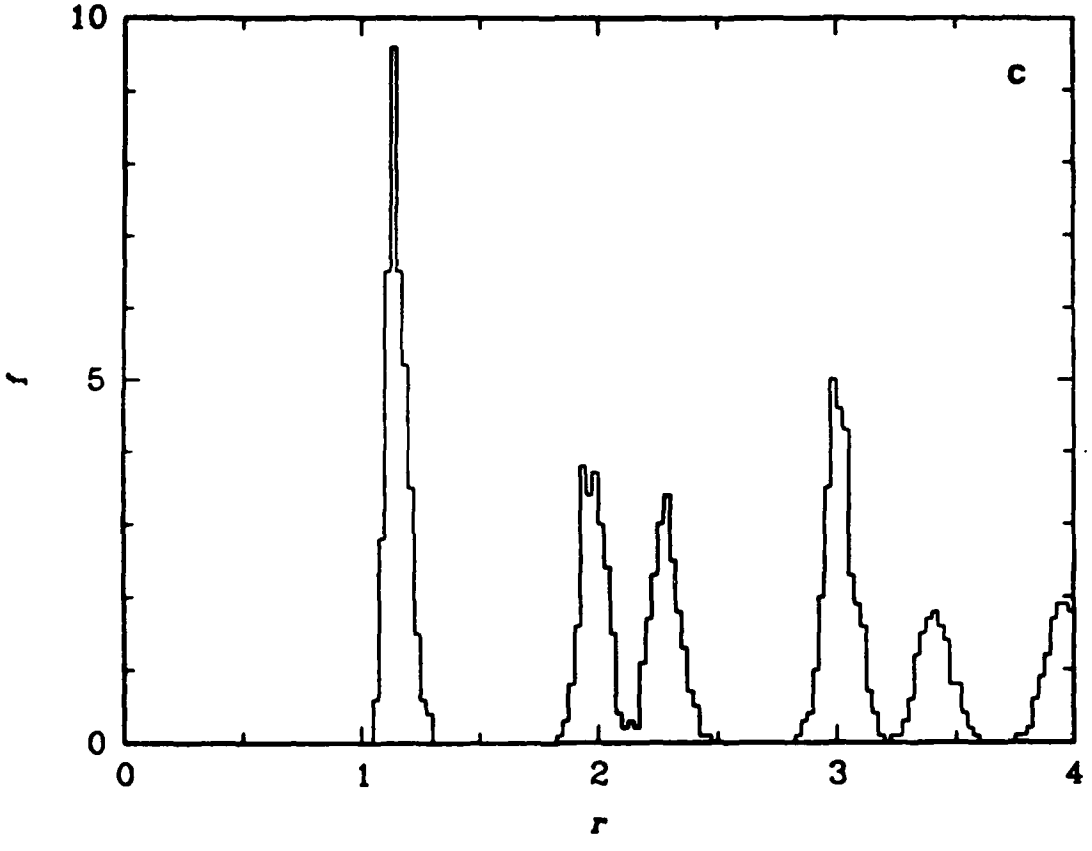

Fig. 7c

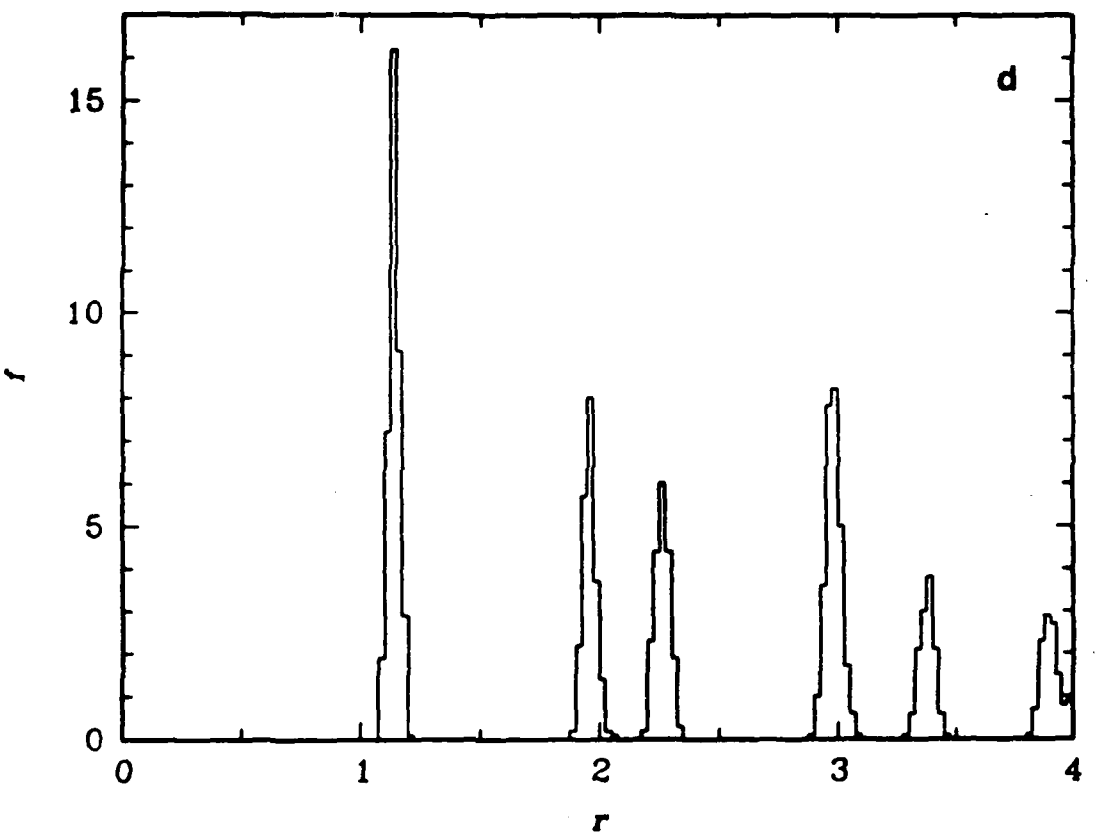

Fig. 7d

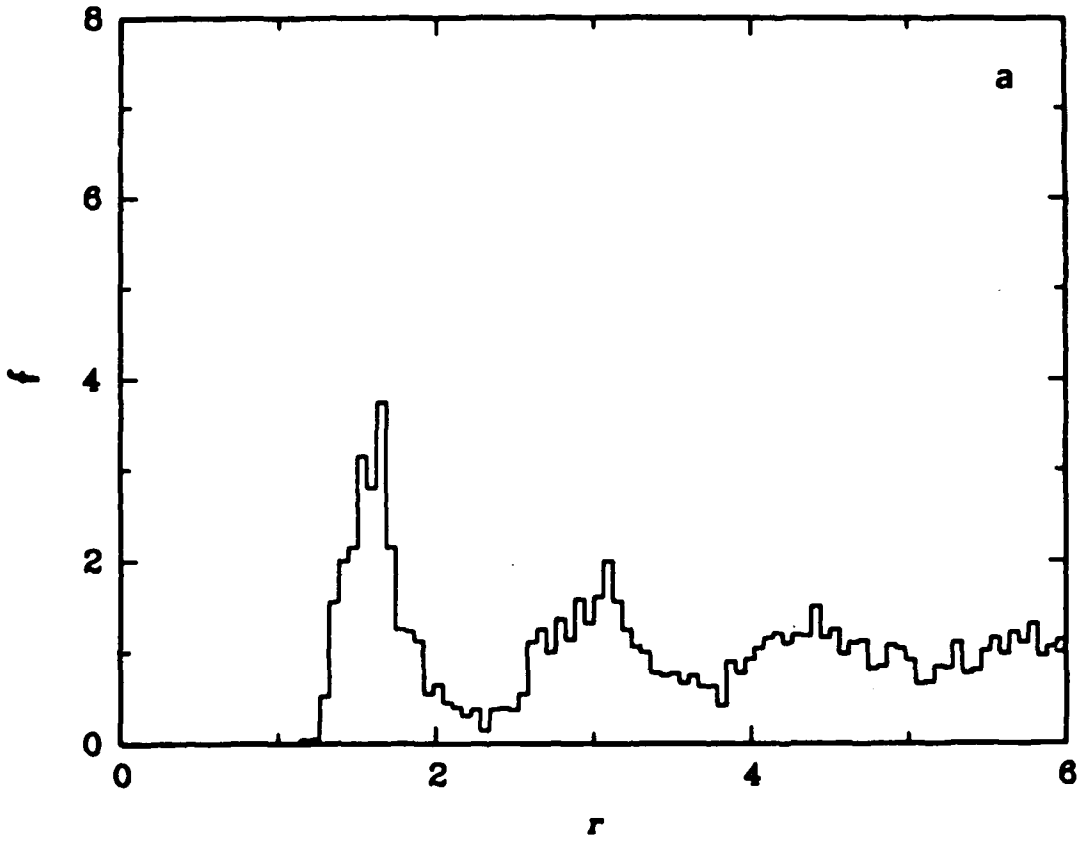

Fig. 8 - Temperature dependent alterations in the RDF in the two-component material below the melting point at an external pressure of $p^* = 1.0$: (a) $T^* = 0.24$, (b) $T^* = 0.14$, and (c) $T^* = 0.06$.

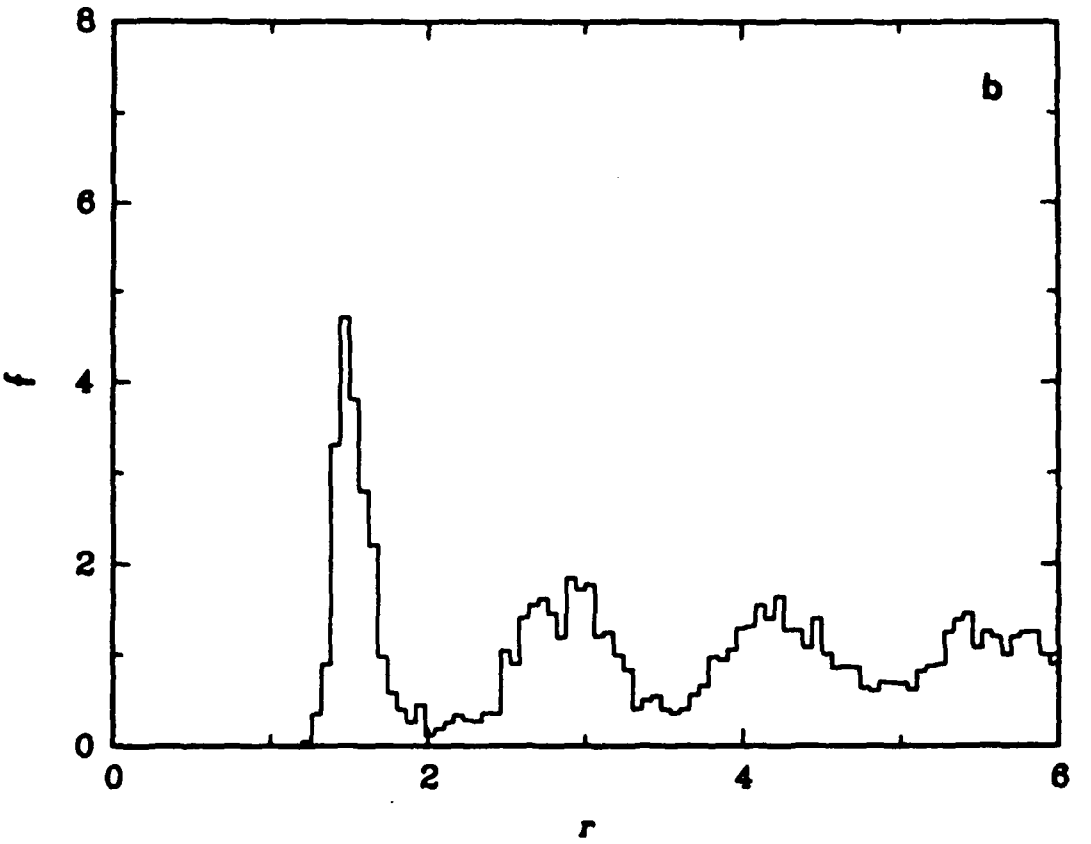

Fig. 8b

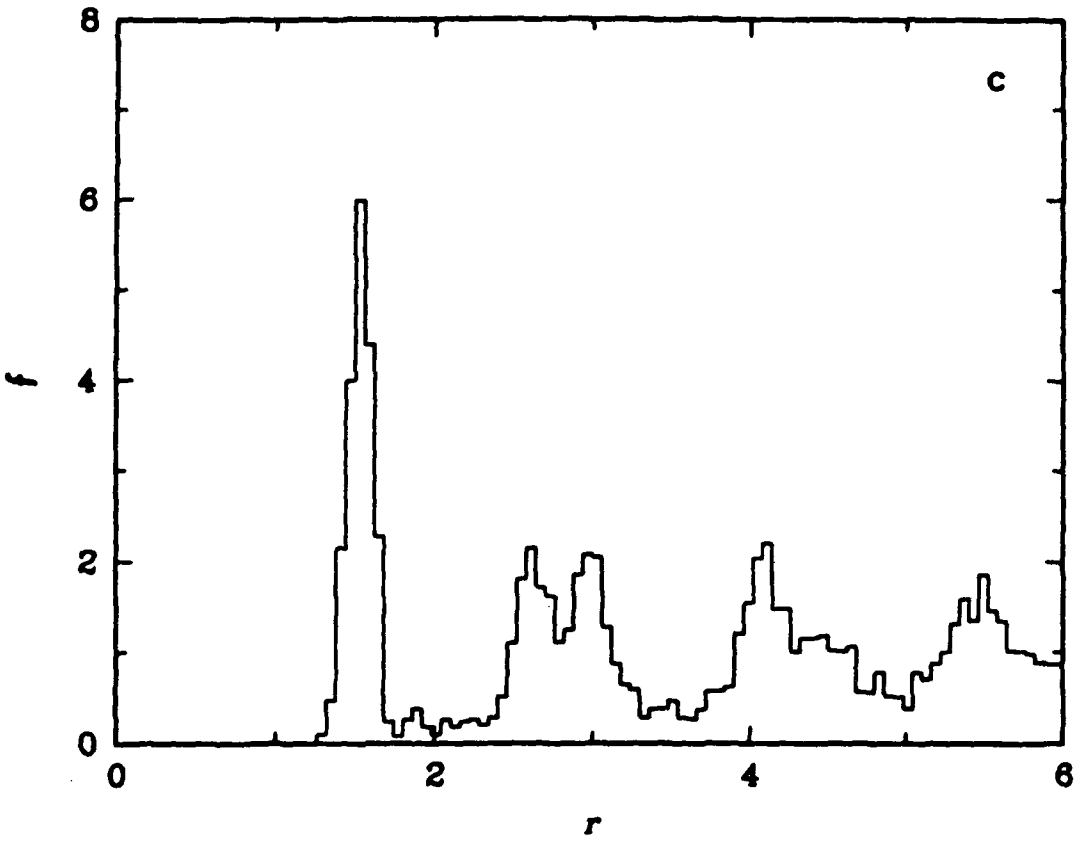

Fig. 8c

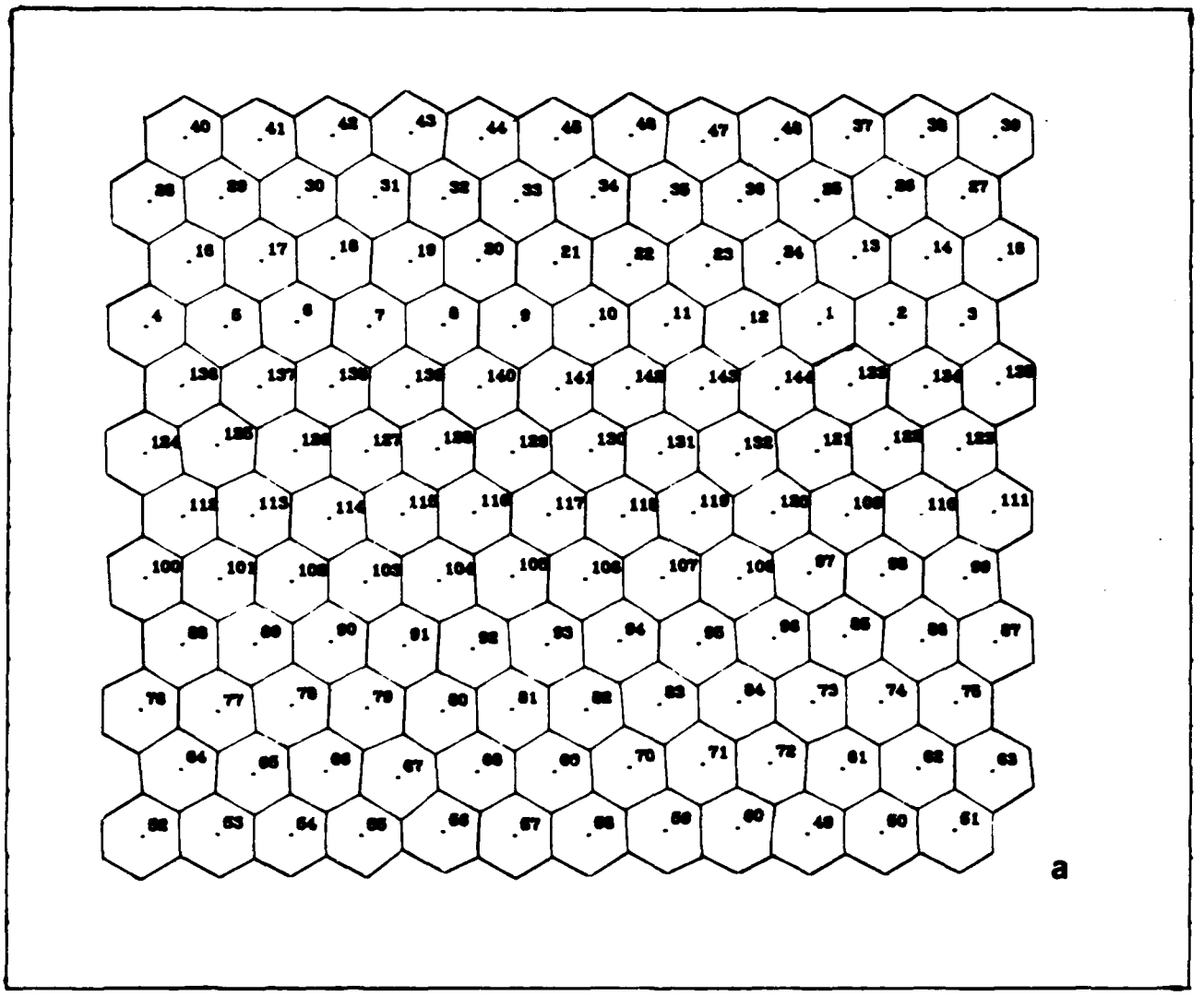

Fig. 9 - Temperature dependent alterations in the structure of the one-component material upon heating at an external pressure of $p^* = 1.0$: (a) $T^* = 0.3$ ($T = 0.5\ T_m$), (b) $T^* = 0.5$, (c) $T^* = 0.6$ ($T = T_m$), incomplete melting after only 10^3 time steps, and (d) $T^* = 0.6$ ($T = T_m$) complete melting after 4000 time steps.

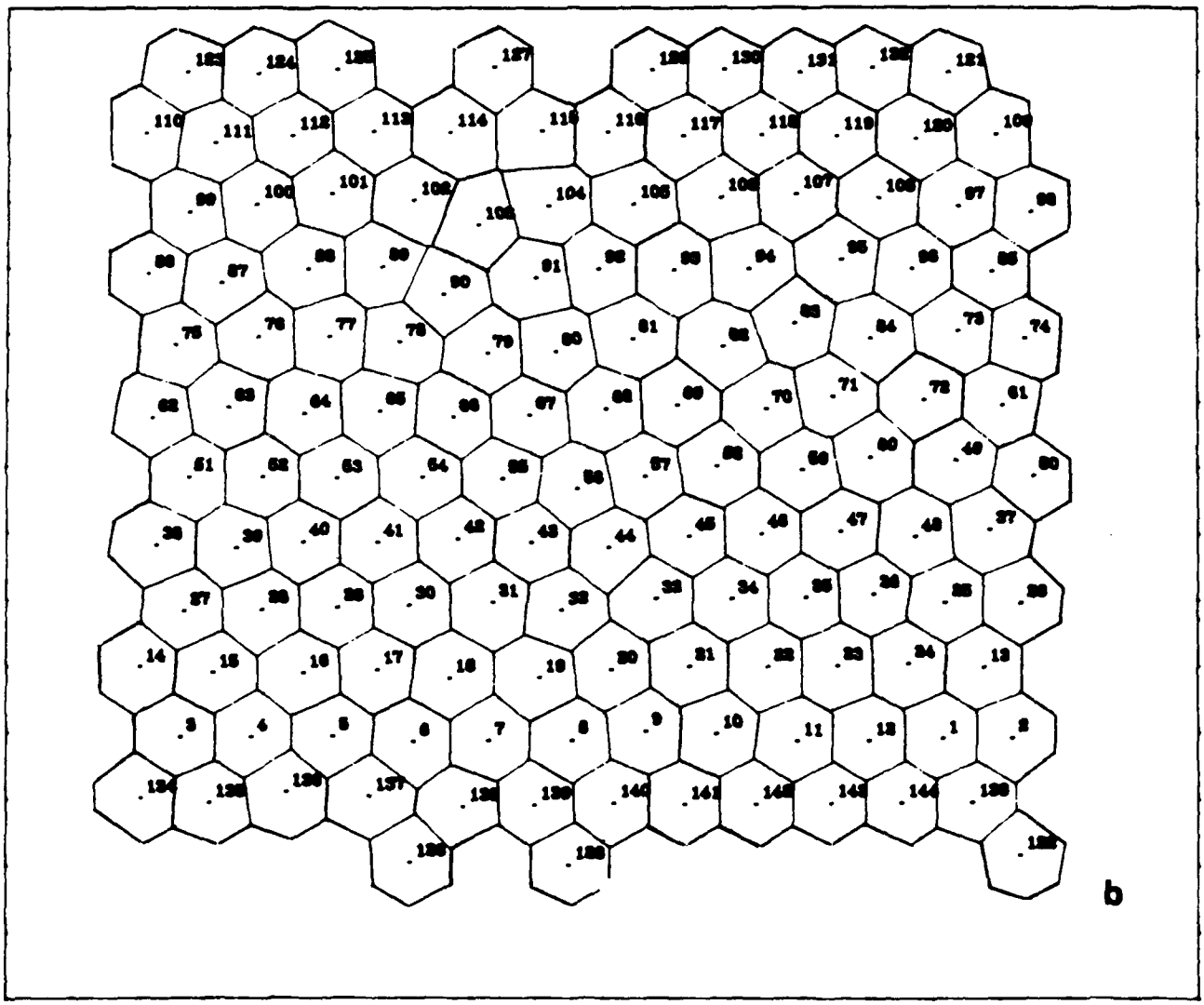

Fig.

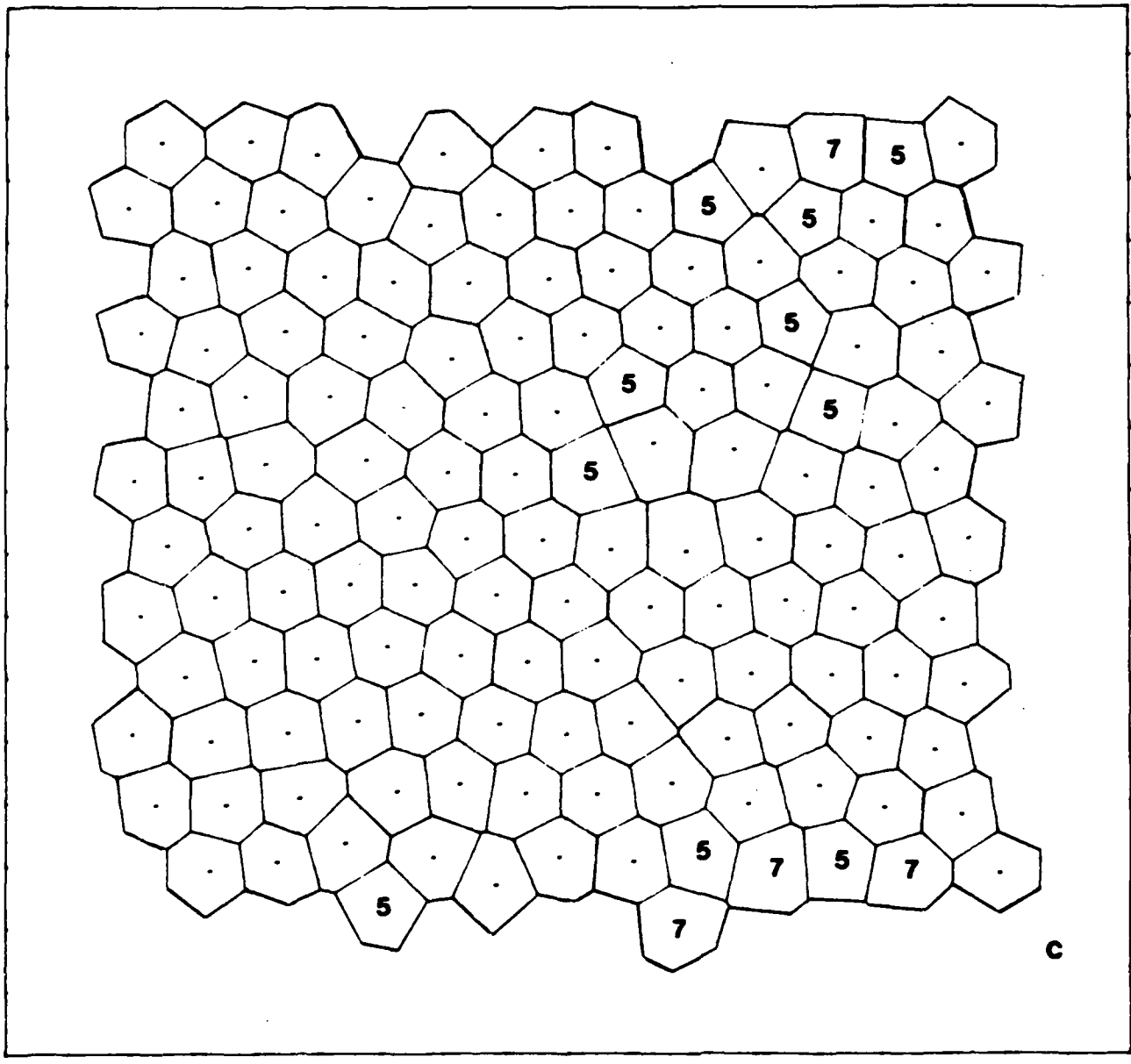

Fig.9c

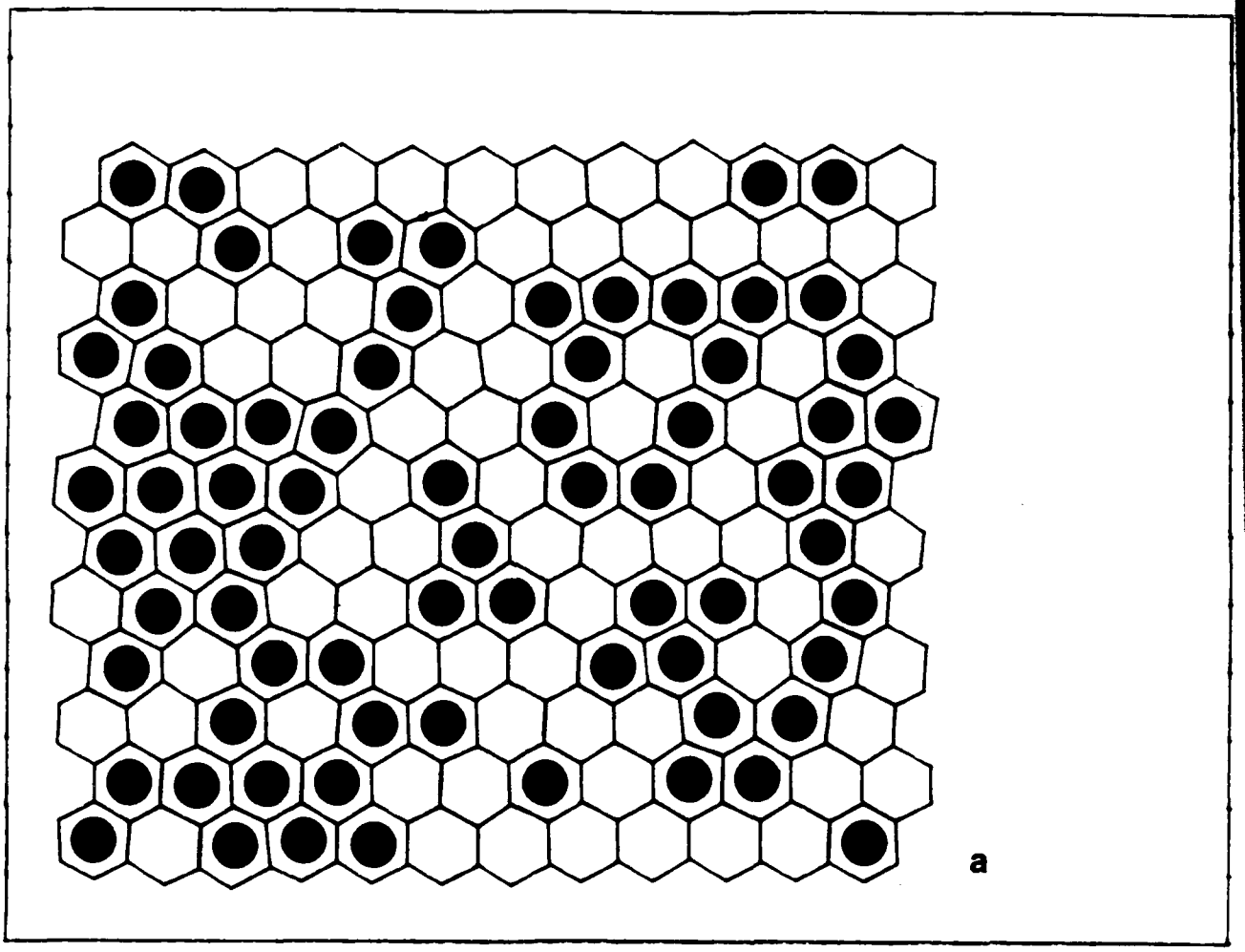

Fig. 10 - Temperature dependent alterations in the structure of the two-component material upon heating at an external pressure of $p^* = 1.0$: (a) $T^* = 0.1$, the dark atoms are Cu, the light ones Zr, (b) $T^* = 0.3$ ($T = T_m$) after complete melting the 5 and 7 sided polygons associate into percolating strings that traverse across the cell.

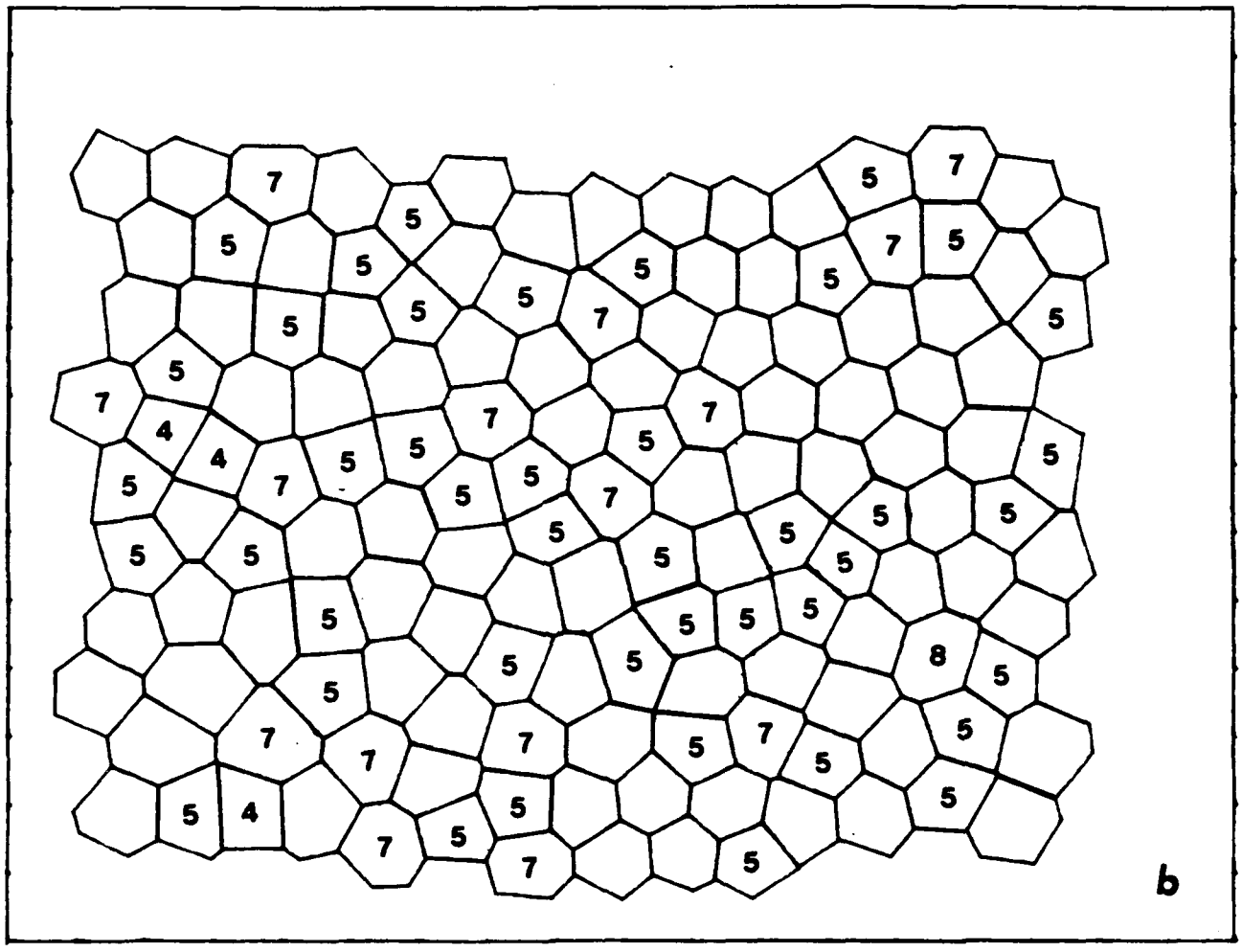

Fig. 10b

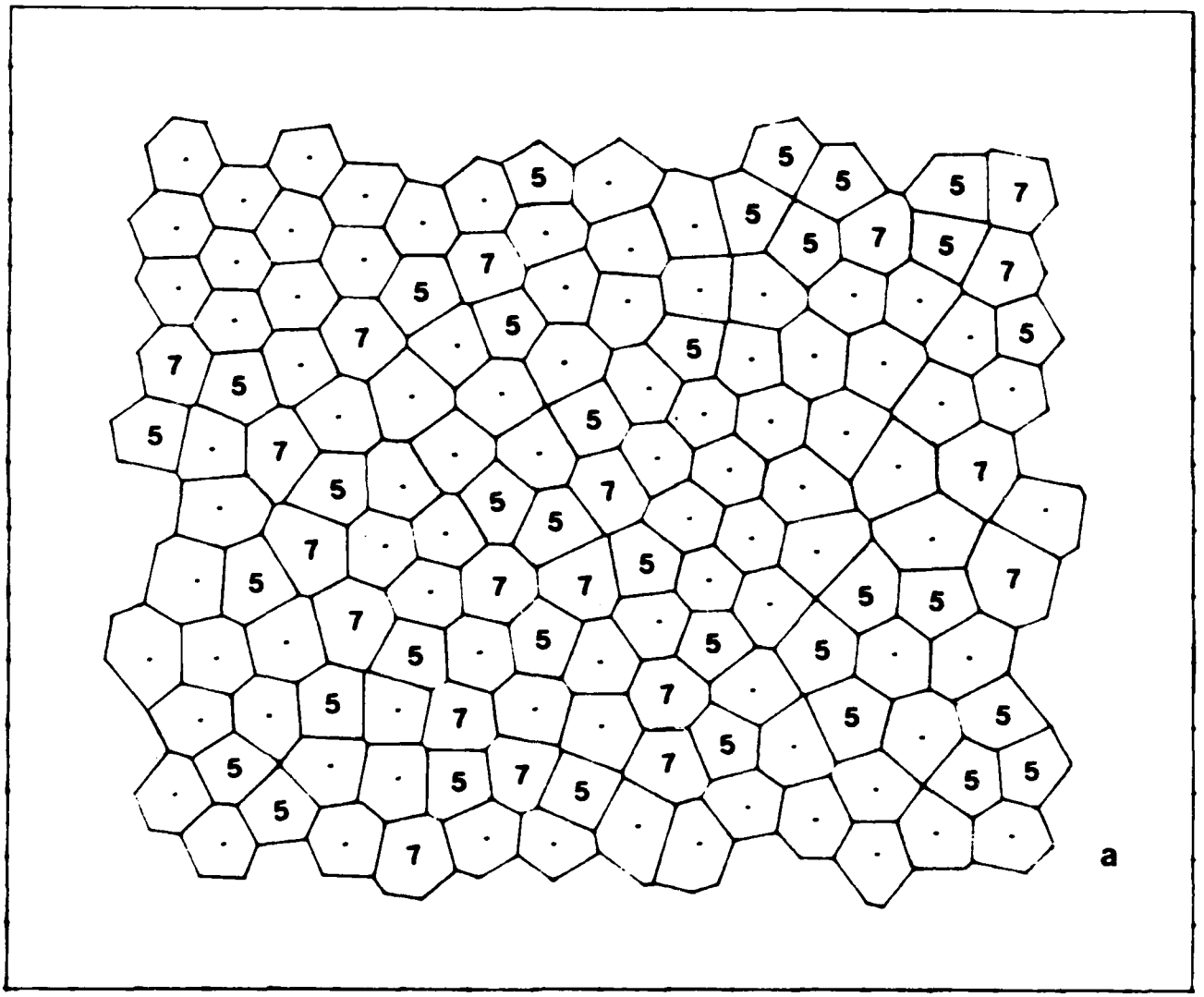

Fig. 11 - Temperature dependent alterations in the structure of the two-component material upon quenching at an external pressure of $p^* = 1.0$: (a) $T^* = 0.3$ ($T = T_m$), (b) $T^* = 0.2$ ($T_g < T < T_m$), (c) $T^* = 0.14$ ($T < T_g$), and (d) $T^* = 0.06$.

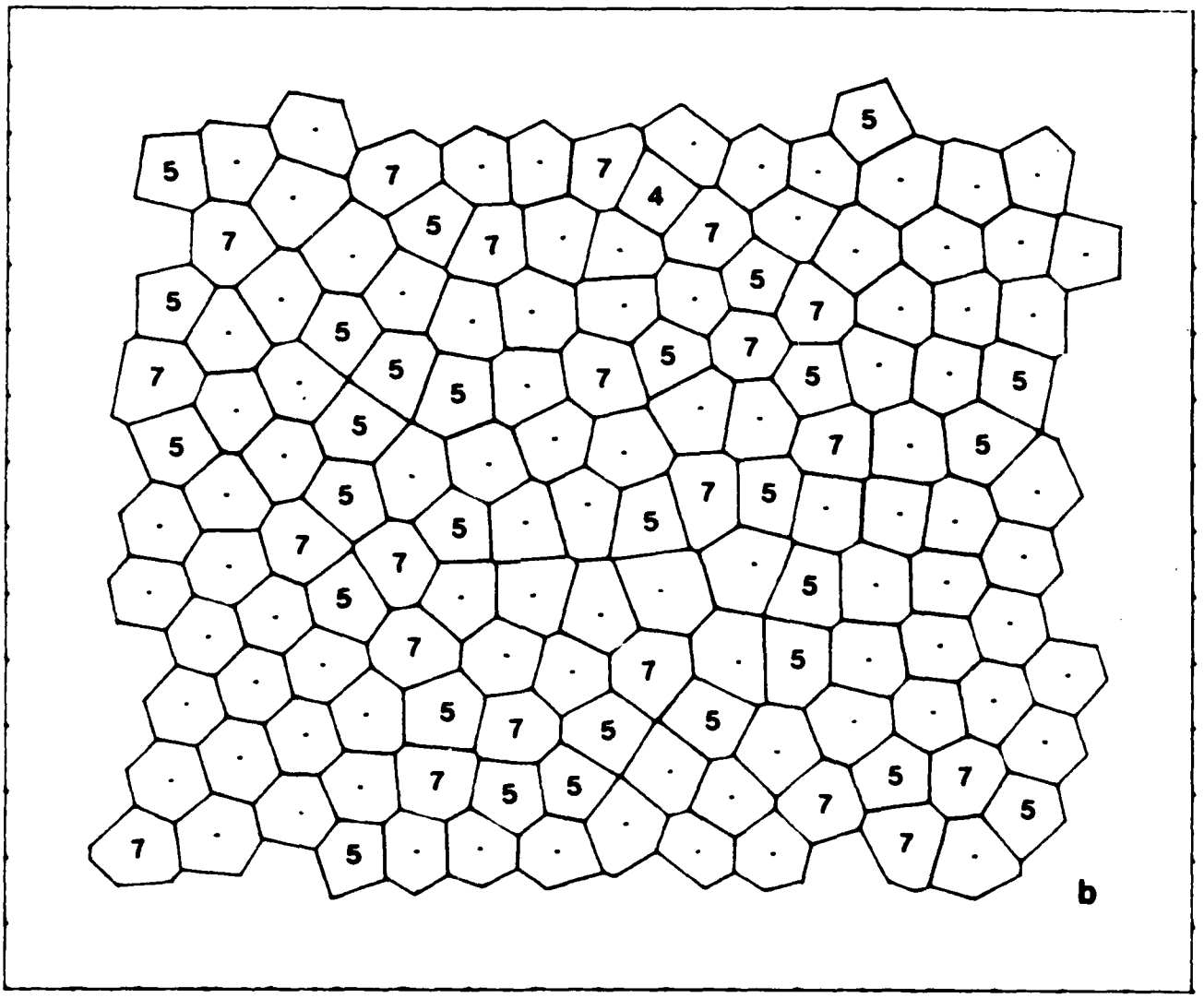

Fig. 11b

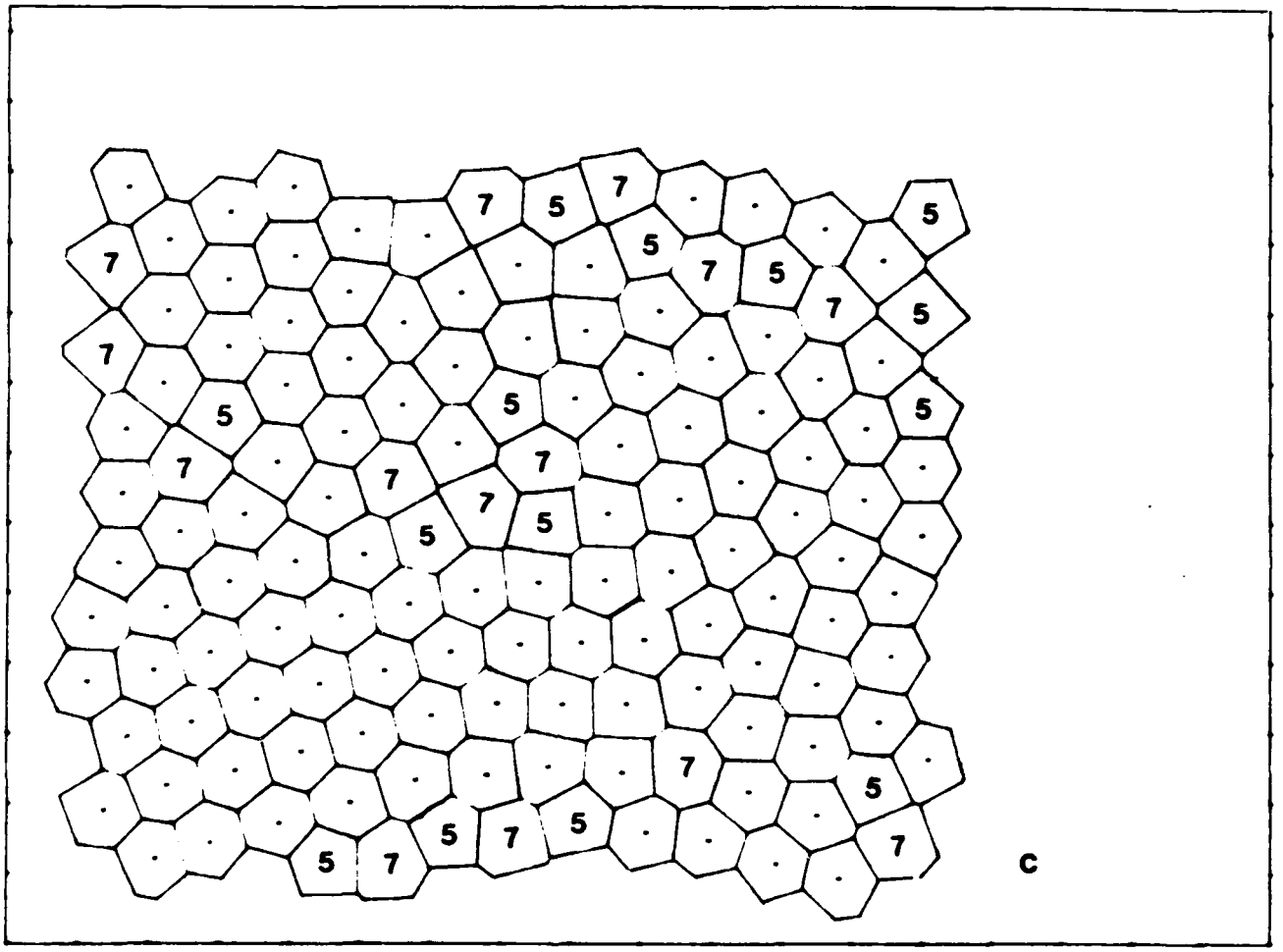

Fig. 11c

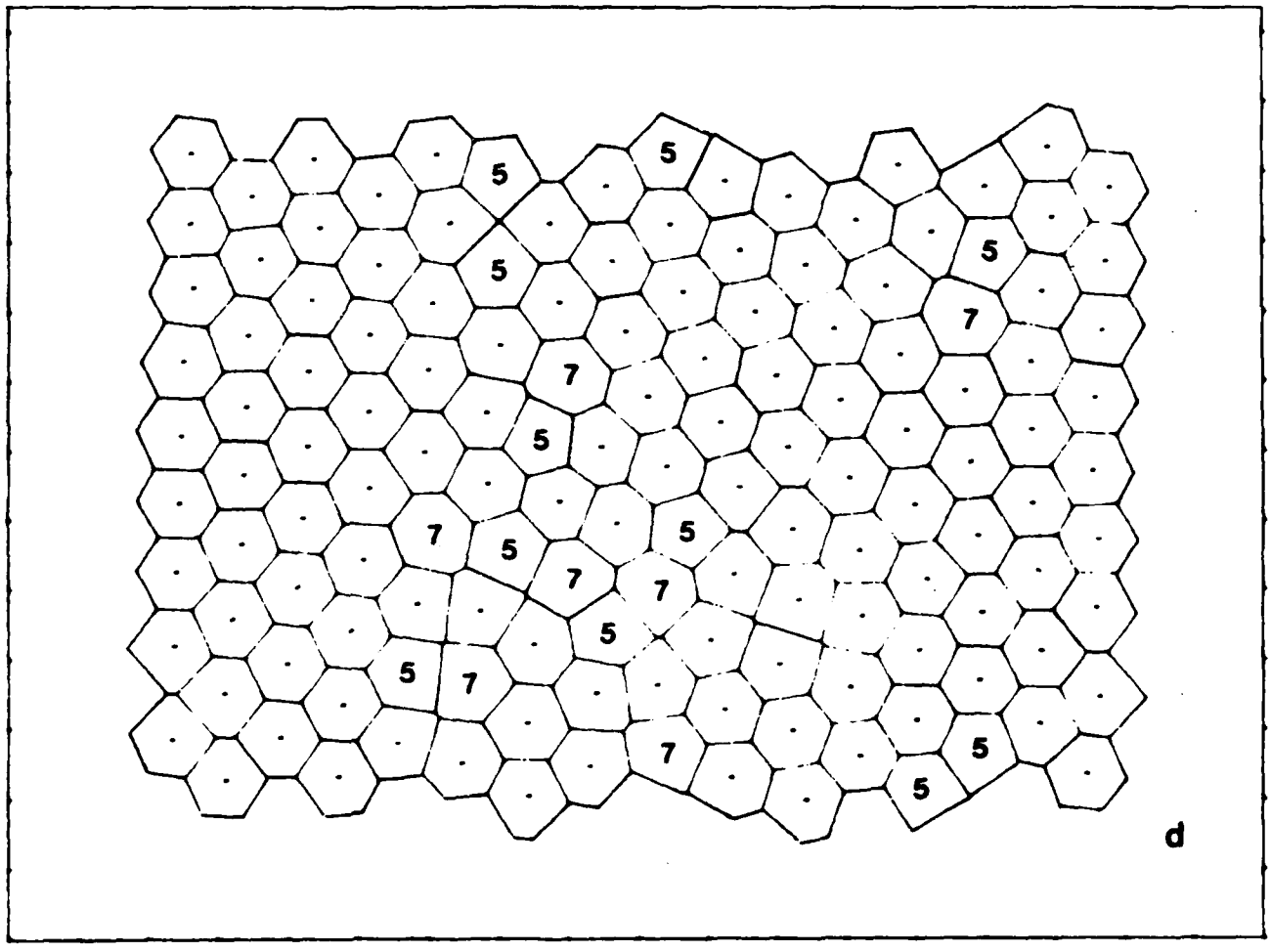

Fig. 11d

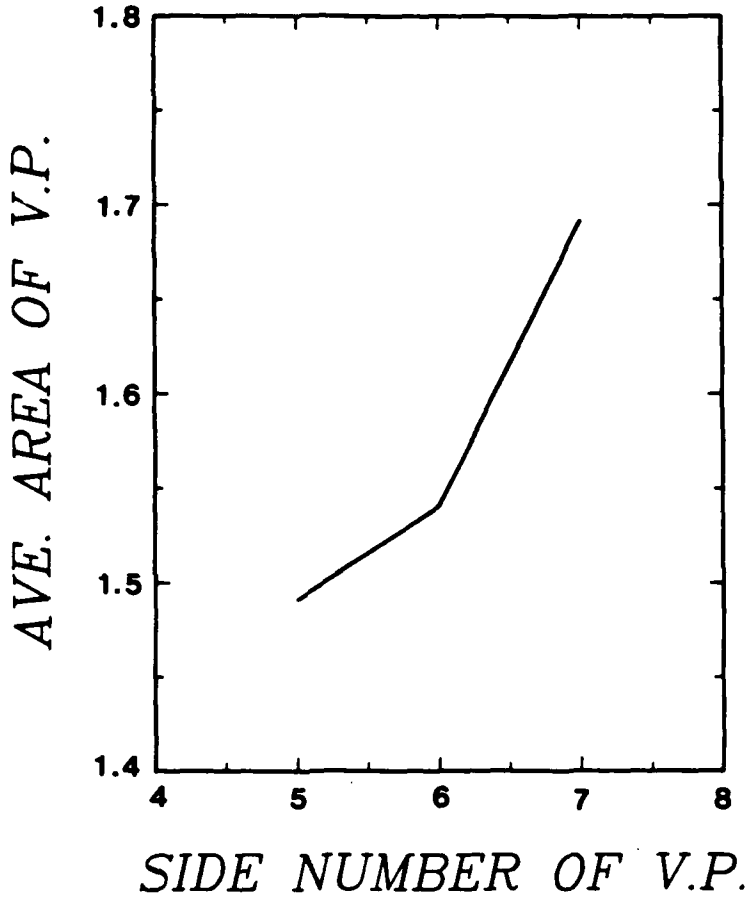

Fig. 12 - Dependence of the average volume of the Voronoi polygons on the number of sides of the polygons, in the two-component material at $T^* = 0.1$.

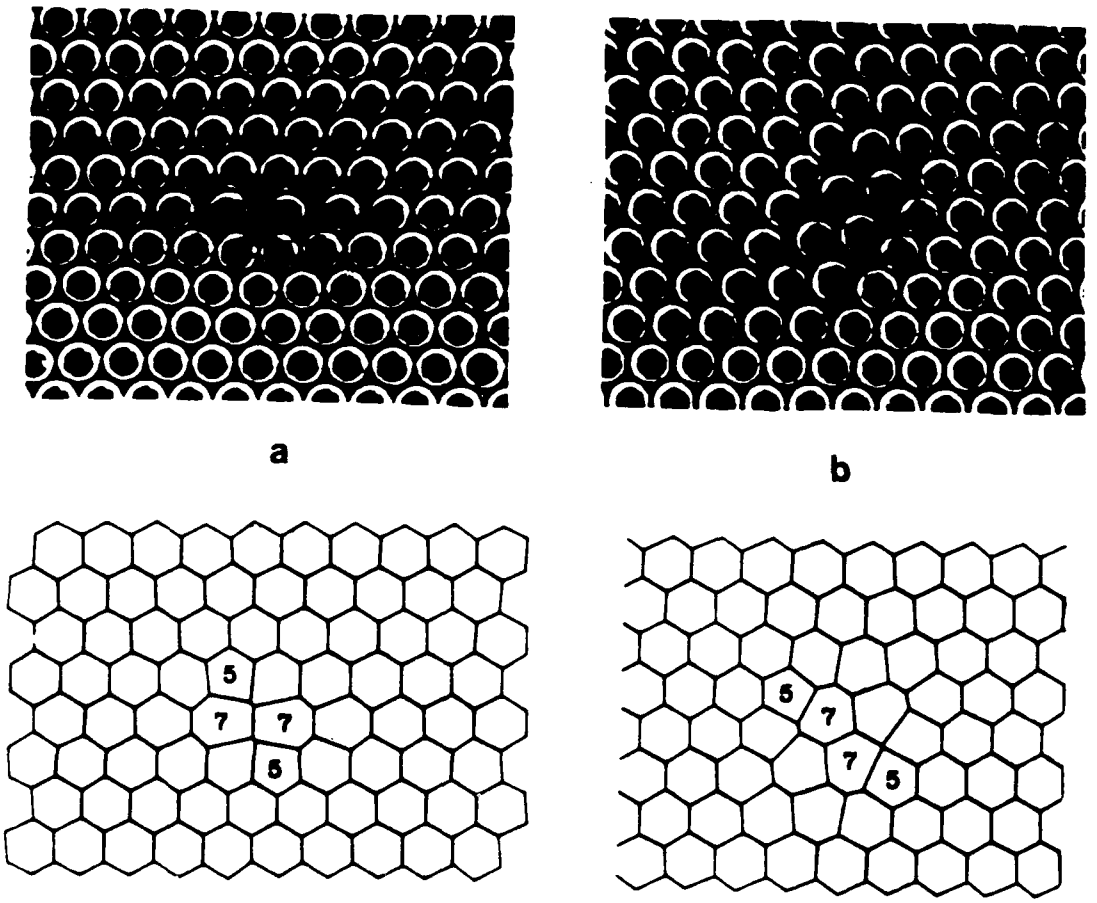

Fig. 13 - Distortions produced in the Voronoi polygon field of a perfect hexagonal bubble raft produced by specific vacancy clusters: (a) vacancy, (b) di-vacancy, (c) tri-vacancy, and (d) quadri-vacancy.

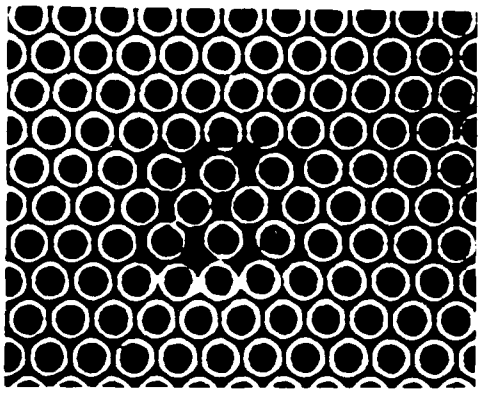

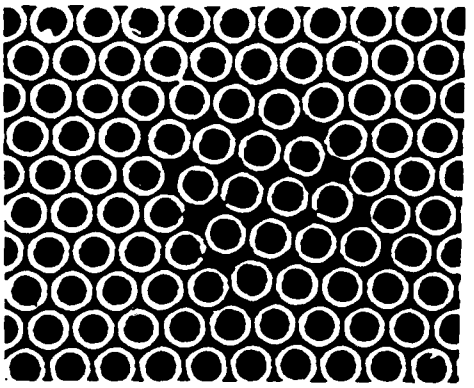

c

d

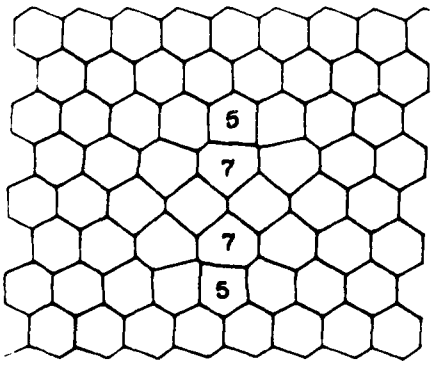

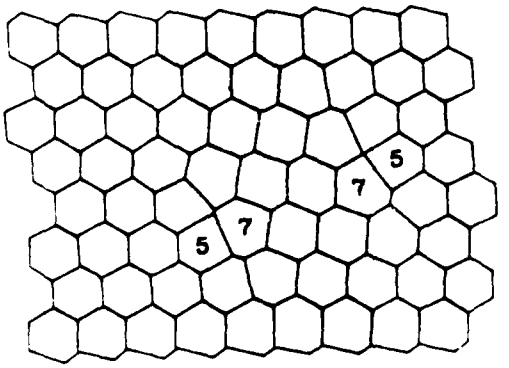

Figs. 13c & 13d

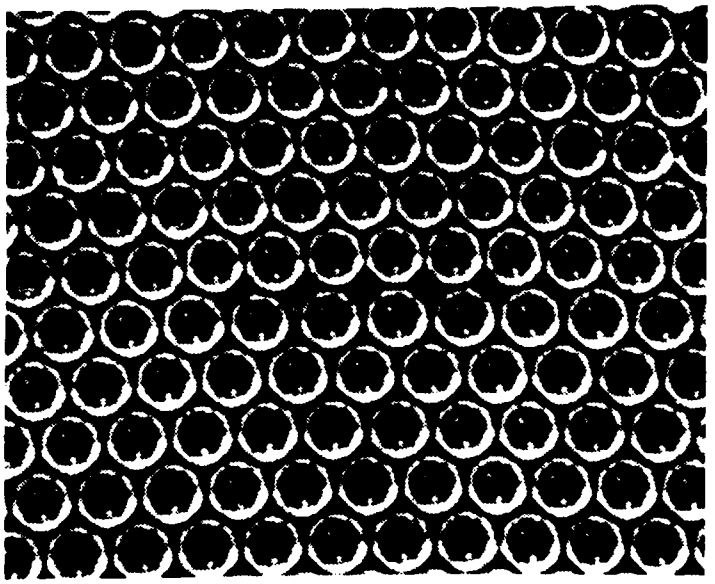

a

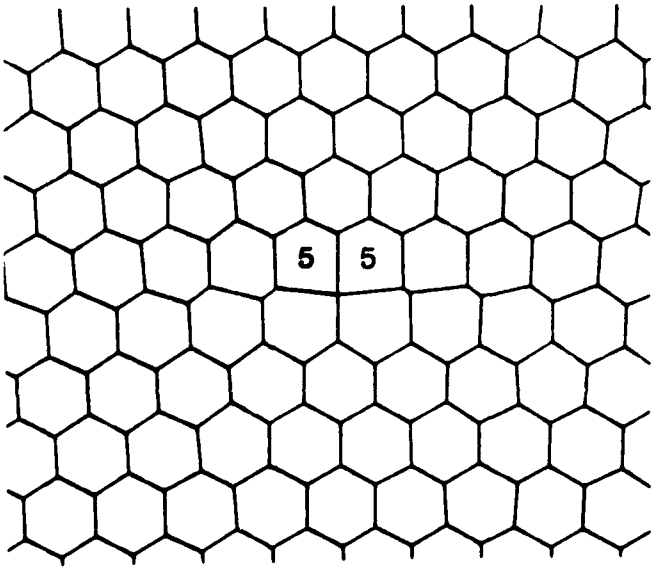

Fig. 14 - Distortions produced in the Voronoi polygon field of a perfect hexagonal bubble raft produced by edge dislocations: (a) edge dislocation in an intermediate position between two low energy configurations, and (b) edge dislocation in the low energy configuration.

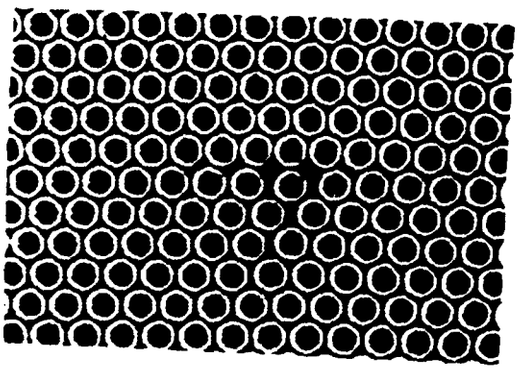

b

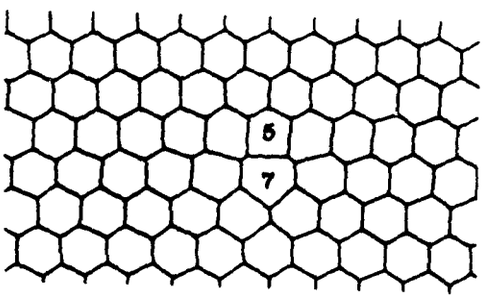

Fig. 14b

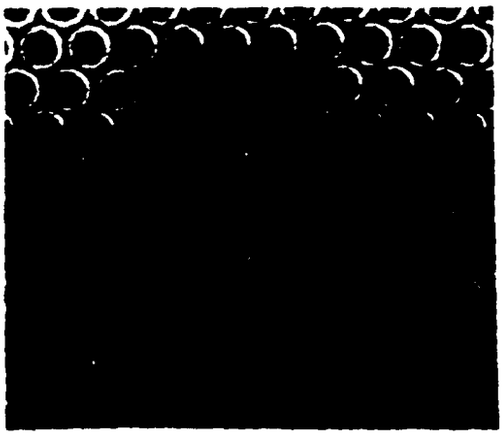

a

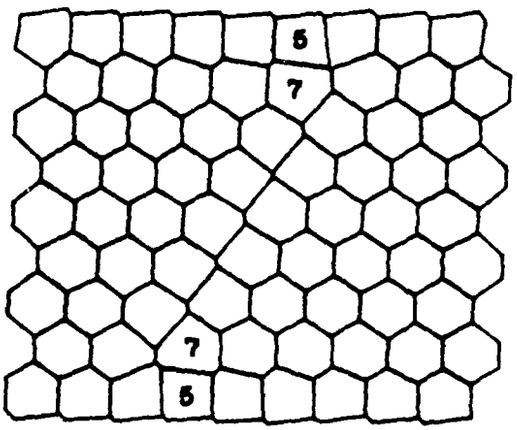

Fig. 15 - (a) A stacking fault with two terminating partials in a perfect hexagonal bubble raft, and (b) a complex two-dimensional fault.

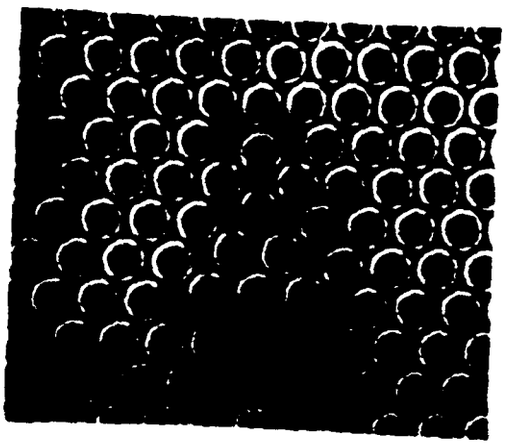

b

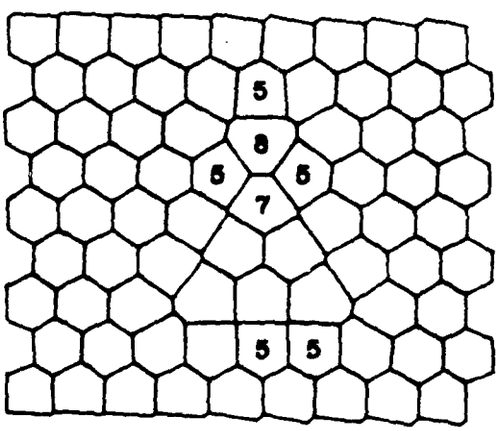

Fig. 15b

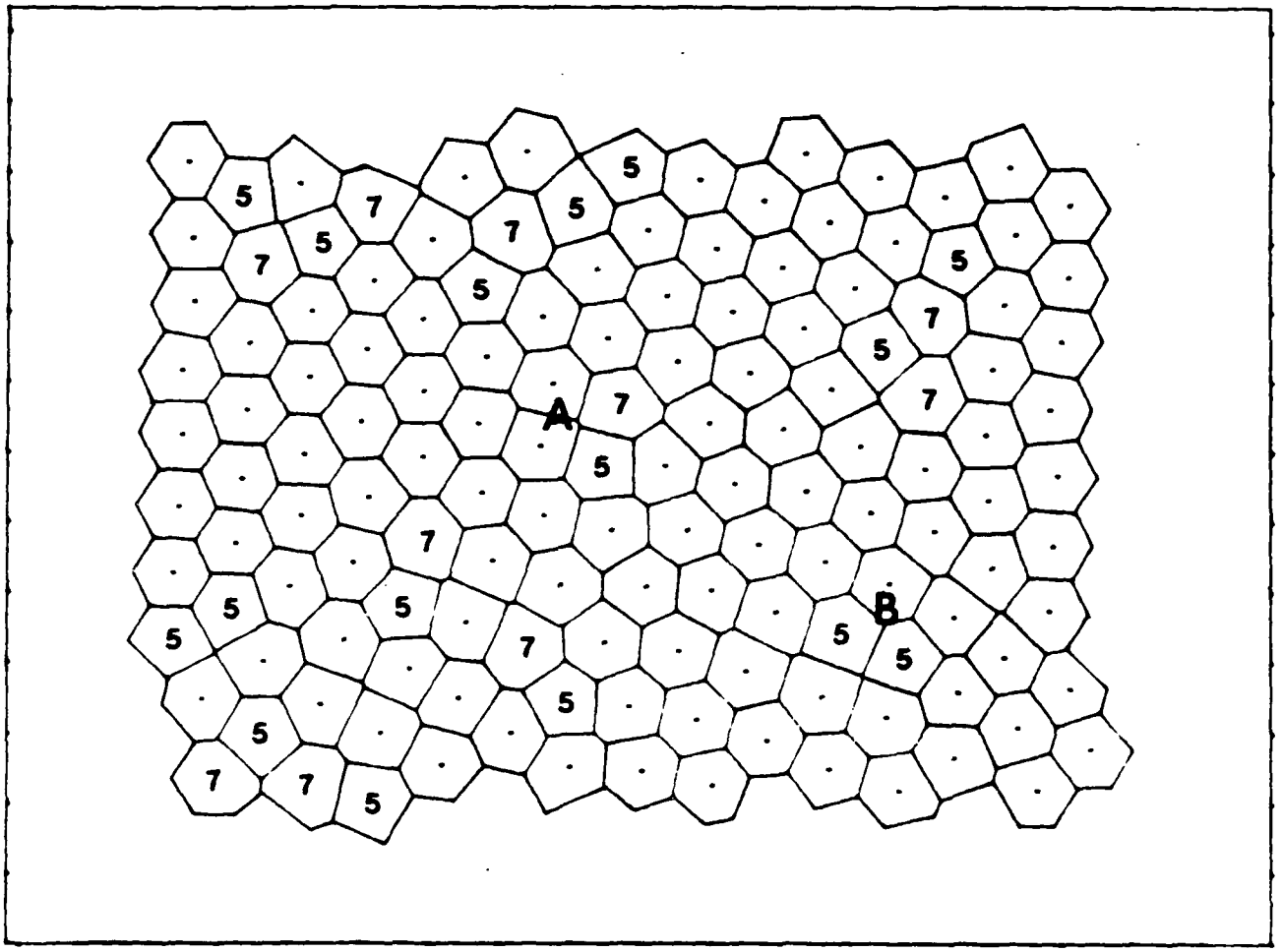

Fig. 16 - Some isolated edge dislocations (5-7 sided dipoles) in a well relaxed two-component glass.